

The converging flow of viscoplastic fluid in a wedge or cone

Jesse J. Taylor-West^{1,†} and Andrew J. Hogg¹

¹School of Mathematics, University of Bristol, Woodland Road, Bristol BS8 1UG, UK

(Received 2 November 2020; revised 19 January 2021; accepted 1 February 2021)

Converging flows of viscoplastic fluids, driven steadily through wedges and axisymmetric cones, are studied analytically and numerically. When the yield stress is relatively large, the bulk of the fluid flows plastically apart from within thin layers where the fluid is strongly sheared in order to achieve no slip at the boundary. Conversely, when the yield stress is relatively small, the motion is viscously dominated with weak corrections to the velocity and stress fields due to viscoplastic effects. For both regimes, viscoplasticity induces a weak angular velocity, directed away from the boundaries, and purely radial flow is not possible. The structure of the flow is calculated using asymptotic methods, confirmed by finite element numerical simulations. Flows of both Bingham and Herschel–Bulkley fluids are analysed, and both planar and axisymmetric geometries are considered. Although these cases differ in their details, they share the same qualitative structure. In particular, the viscoplastic boundary layers that emerge when the yield stress is relatively large, ensure not only that no slip is enforced, but also, through an intermediate matching layer, that the shear rates remain bounded.

Key words: boundary layer structure, non-Newtonian flows, low-Reynolds-number flows

1. Introduction

The steady flow of a viscous fluid in a planar wedge is a fundamental problem in fluid mechanics (Drazin & Riley 2006). First documented by Jeffery (1915) and Hamel (1917), the flow is a rare example of a general solution to the Navier–Stokes flow at all Reynolds numbers. ‘Jeffery–Hamel flow’ has been studied extensively (see, for e.g. Dean 1934; Rosenhead 1940; Fraenkel 1962; Banks, Drazin & Zatorska 1988). For convex wedges, with half-angle $\alpha \leq 90^\circ$, converging and diverging solutions exist at vanishing Reynolds numbers for all wedges, while at larger Reynolds numbers the flow forms thin boundary layers at the walls. These layers are stable for converging flow but unstable for diverging flow, resulting, above a critical Reynolds number, in separation, and the formation of a

[†] Email address for correspondence: j.taylor-west@bristol.ac.uk

central jet and regions of reversed flow at the walls. In essence this occurs because the weak viscous stresses are unable to balance the adverse pressure gradient of the diverging flow.

Steady converging flows of plastic materials also have a long history. Nadai (1924) derived a solution for the converging flow of a perfectly rigid plastic in a wedge, with a constant friction imposed on the walls (solution presented in English by Hill 1950), and Shield (1955) solved the corresponding problem in an axisymmetric conical geometry. Notably, both of these flow solutions exhibit slip and divergent shear rates at the boundaries. Motivated by industrial applications such as wire drawing, polymer processing, extrusion of pastes and the discharge of granular materials from hoppers and silos, more recent studies have examined the converging flows of other non-Newtonian fluids. For example, the slow converging flow of incompressible power-law fluids has been studied by Durban (1986), Brewster *et al.* (1995) and Nagler (2017), while the viscoelastic problem has been studied by Hull & Pearson (1984). The work by Brewster *et al.* (1995) is of particular interest, as they consider a power-law fluid of small shear exponent, for which they construct similarity solutions under the assumption of purely radial flow, and demonstrate the need for a complex boundary layer structure in order to enforce no slip at the walls.

Viscoplastic fluids are a particular class of non-Newtonian fluid which act as a rigid plastic or flow as a viscous fluid, depending on whether the stress is less than or exceeds a critical yield stress, respectively. This behaviour is common for slurries and suspensions, and the viscoplastic model has wide ranging applications in geophysics and industry (Ancy 2007; Balmforth, Frigaard & Ovarlez 2014; Frigaard, Paso & de Souza Mendes 2017). The non-Newtonian behaviour is characterised by the dimensionless Bingham number, Bi , which measures the magnitude of the yield stress to the viscous stresses developed by the flow. (The precise definition of Bi for the flow analysed in this study is given in (2.13).)

For the slow converging flow of a viscoplastic fluid, Cristescu (1975) studied the stress distribution produced by a given kinematically feasible radial velocity profile in a cone, without attempting to solve the full system of partial differential equations required to explicitly determine the coupled velocity and stress fields. Motivated by strip drawing in the regime of low yield stress or fast drawing speed, Sandru & Camenshi (1979) analysed the converging flow of a viscoplastic material when the Bingham number was relatively small. They imposed ‘friction’ boundary conditions in the form of an imposed ratio between shear and normal stresses at the boundaries. No-slip boundary conditions can be treated as the limiting case of this approach, in which the deviatoric normal stress vanishes and the shear stress is maximised. Although this case was not the focus of Sandru & Camenshi (1979) and they stop short of explicit evaluation of the velocity fields, we demonstrate that their perturbation solution may be used to calculate the velocity fields and, in particular, emphasise that the solution implies purely radial flow is not possible. Durban (1984, 1985, 1986) calculated flow profiles and stress fields for both a planar wedge and an axisymmetric conical die, under constant friction boundary conditions, as opposed to no-slip boundary conditions. These results are restricted by the assumption that the wall friction is low compared to the yield stress, as relevant to well lubricated, metal-forming processes at high temperatures, and the flow profiles are assumed to be purely radial and approximately uniform. Later, Alexandrov, Lyamina & Mishuris (2007) studied viscoplastic flow in a wedge under maximum friction boundary conditions, their definition of which reduces to the condition that the deviatoric stress consists only of shear stresses at the wall. Under this boundary condition they find that the radial velocity must be

constant at the boundary, which is inconsistent with a slipping regime in which the radial velocity increases towards the vertex of the wedge. They further consider constitutive laws with a saturation stress (where the stress remains bounded as strain rates diverge) and find that the classical assumptions of a radially independent stress state and purely radial flow are inconsistent when shear stresses become comparable to the shear yield stress. They identify the cause of these difficulties as the divergent strain rates that occur at the wall in the perfectly plastic solution. However, they do not attempt to derive velocity or stress fields for either the standard viscoplastic model, or for one with a saturation stress. Finally, Ara *et al.* (2019) recently performed a numerical study of wedge flow of a Bingham fluid including heat transfer, in the presence of a magnetic field. Again, this study assumed a purely radial flow to derive ordinary differential equations for similarity solutions. These solutions are found to be dependent on radius through the authors' definition of Bingham number, and so the conclusions of this work rely on an implicit assumption that this radial dependence is sufficiently weak to be neglected in the expression of conservation of mass.

In this paper, we present a comprehensive analysis of converging flow of viscoplastic fluid through a wedge or cone, that satisfies no-slip boundary conditions, in both the plastically ($Bi \gg 1$) and viscously ($Bi \ll 1$) dominated regimes. We initially carry out a full analysis for a Bingham fluid in a planar wedge, before extending the theory to a Herschel–Bulkley fluid in a wedge and a Bingham fluid in an axisymmetric conical geometry, both of which share the same analytical framework to the flow of a Bingham fluid through a wedge, but are algebraically more involved. Most importantly, in all cases we find that the viscoplasticity introduces a weak angular flow towards the centre of the wedge or cone, explaining the challenges faced by previous attempts to find purely radial solutions. Furthermore, in the plastically dominated regime, boundary layers are found at the wall, allowing the solution to satisfy no slip. The angular extent of these boundary layers is found to decrease with Bingham number as $Bi^{-1/2}$ (or $Bi^{-1/(N+1)}$ for a Herschel–Bulkley fluid of flow index N) and depends also on the radial distance from the apparent apex of the wedge or cone, r . Direct numerical simulations for a Bingham fluid in a planar wedge are carried out using the finite element method, verifying the analytical results in both regimes.

In the plastic regime, the converging flow field away from the boundaries is given to leading order by the solutions derived by Nadai (1924) and Shield (1955), with viscous effects becoming significant within relatively thin boundary layers in which the shear rates are relatively large and the shear stresses exceed the yield stress. The velocity field in this regime may be determined using viscoplastic boundary layer techniques, originally developed by Oldroyd (1947). Oldroyd explored a distinguished limit in which viscous shear stresses and plastic extensional stresses are both significant in the streamwise momentum balance, which occurs for dimensionless boundary layer widths of order $Bi^{-1/3}$. Viscoplastic boundary layers were re-examined by Piau (2002), who argued for a different distinguished scaling from Oldroyd, in which viscous shear stresses dominate the momentum balance, and boundary layer widths instead scale like $Bi^{-1/2}$. Most recently, Balmforth *et al.* (2017) developed a consistent boundary layer theory for viscoplastic flows, clarifying the conditions under which Oldroyd's and Piau's scalings are appropriate. Specifically, they determined that where the boundary layer is adjacent to a rigid wall, the boundary layer structure is consistent with Piau's arguments (although the exact scaling can vary depending on the far field pressure gradient), whereas when bounded only by unyielded or plastically deforming fluid, the appropriate scaling is Oldroyd's. In the problems studied by Balmforth *et al.* (2017), the boundary layer solutions are only explicitly asymptotically matched to rigid plugs. However, in the problem considered in

this work, the velocity is varying at the outer edge of the boundary layer due to the converging geometry, and thus our asymptotic construction is rather different. It will be shown that the solution does share some similarities with other viscoplastic flows which exhibit regions of nearly plastic deformation, such as flow in an eccentric annulus (Walton & Bittleston 1991), flow around a cylinder (Tokpavi, Magnin & Jay 2008) or thin-layer gravitational flow (Balmforth & Craster 1999). In the weakly yielded regions, or ‘pseudo-plugs’, present in these flows, the second invariant of the deviatoric stress does not exceed the yield stress at leading order, but does so at higher orders. These regions are typically delineated from fully yielded material by ‘fake yield surfaces’. In accord with the previous results for viscoplastic boundary layers, we show that the width of the layer scales like $Bi^{-1/2}$, as expected for flow bounded by rigid walls, but that it is matched, via an intermediate asymptotic layer encompassing a fake yield surface, to a weakly yielded, pseudo-rigid plastic solution in the bulk of the wedge. The existence of these two asymptotic layers is a consequence of the need to both impose no slip and to regularise the divergent shear rates found at the wall in the rigid plastic solution of Nadai (1924).

We first define the problem and outline the solution for the converging wedge flow of a Bingham fluid (§ 2). We then construct the asymptotic solution for the plastic regime and compare the results to direct numerical simulations (§ 3). The asymptotic solution for the viscous regime is derived and compared to direct simulations in § 4. We focus initially on the Bingham fluid and planar geometry, since this case most clearly demonstrates the asymptotic structure with minimal algebraic complications. We then generalise the problem to a Herschel–Bulkley fluid (§ 5), and to an axisymmetric conical geometry (§ 6), which both follow the same asymptotic structure as the solutions in §§ 3,4, but are algebraically more involved due to rheology (§ 5) and geometry (§ 6). We summarise and conclude our study in § 7. There are also four appendices in which we provide some of the algebraic details required for the derivation of the flow solutions.

2. Problem definition: Bingham fluid in a planar wedge

We analyse steady slow incompressible flow of a viscoplastic fluid through a planar wedge of half-angle α (see figure 1). We restrict our focus to $\alpha \leq \pi/2$, for which the geometry represents a converging flow in a wedge, as opposed to a sink flow external to a wedge when $\alpha > \pi/2$. A volume flux per unit width, Q (taken to be positive for flow towards the vertex), is imposed and we assume that the wedge is sufficiently long that end effects may be ignored. The flow field is predominantly in the radial direction and is assumed symmetric about the centre-line of the wedge. Plane polar coordinates, (r, θ) , are defined relative to the apparent vertex of the wedge. The key dependent variables are the velocities in the radial and angular directions, denoted by u and v respectively.

We initially assume the constitutive law for a Bingham fluid, before generalising to the Herschel–Bulkley model in § 5. Thus, the constitutive law is given by

$$\begin{cases} \begin{pmatrix} \tau_{rr} \\ \tau_{r\theta} \end{pmatrix} = \left(\mu + \frac{\tau_c}{\dot{\gamma}} \right) \begin{pmatrix} \dot{\gamma}_{rr} \\ \dot{\gamma}_{r\theta} \end{pmatrix} & \text{if } \tau > \tau_c, \\ \dot{\gamma} = 0 & \text{otherwise,} \end{cases} \quad (2.1)$$

where μ is the Bingham plastic viscosity and τ_c is the yield stress. The variables $(\tau_{rr}, \tau_{r\theta})$ and $(\dot{\gamma}_{rr}, \dot{\gamma}_{r\theta})$ are the components of the deviatoric stress and strain-rate tensors,

The converging flow of viscoplastic fluid

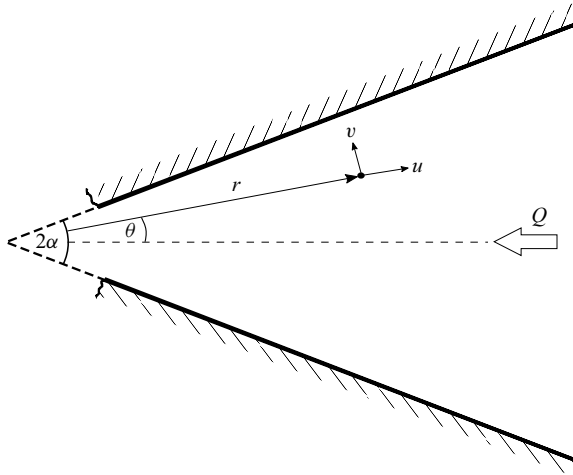


Figure 1. A schematic of the flow geometry.

respectively, τ and $\dot{\gamma}$ are the corresponding second invariants given by

$$\dot{\gamma}^2 = \dot{\gamma}_{rr}^2 + \dot{\gamma}_{r\theta}^2 \quad \text{and} \quad \tau^2 = \tau_{rr}^2 + \tau_{r\theta}^2, \quad (2.2a,b)$$

and the strain-rate tensor is defined by

$$\dot{\boldsymbol{\gamma}} = (\nabla \mathbf{u}) + (\nabla \mathbf{u})^T, \quad (2.3)$$

where \mathbf{u} is the velocity vector and T is the transpose. Due to the flow convergence we expect that $\dot{\gamma} > 0$, and hence that the fluid is yielding everywhere and rigid plugs do not form in the flow. As such, we need only consider the $\tau > \tau_c$ case of the constitutive law (2.1).

We have the following dimensional quantities in our problem: density, ρ , viscosity, μ , yield-stress, τ_c , volume flux per unit width, Q , and typical radial distance from the vertex, R . We scale velocities by Q/R , strain rates by Q/R^2 , stresses and pressures by $\mu Q/R^2$ and, unless stated otherwise, all variables will be assumed dimensionless. On the further assumption that the flow is sufficiently slow to ignore inertial effects, the non-dimensional governing equations in polar coordinates are given by

$$\frac{1}{r} \frac{\partial (ru)}{\partial r} + \frac{1}{r} \frac{\partial v}{\partial \theta} = 0, \quad (2.4)$$

$$\frac{\partial p}{\partial r} = \frac{\partial \tau_{rr}}{\partial r} + \frac{1}{r} \frac{\partial \tau_{r\theta}}{\partial \theta} + \frac{2}{r} \tau_{rr}, \quad (2.5)$$

$$\frac{1}{r} \frac{\partial p}{\partial \theta} = \frac{\partial \tau_{r\theta}}{\partial r} - \frac{1}{r} \frac{\partial \tau_{rr}}{\partial \theta} + \frac{2}{r} \tau_{r\theta}, \quad (2.6)$$

which express incompressibility (2.4) and the balance of momentum in the radial (2.5) and angular (2.6) directions. The deviatoric stress and strain-rate tensors are given by

$$\begin{pmatrix} \tau_{rr} \\ \tau_{r\theta} \end{pmatrix} = \left(1 + \frac{Bi}{\dot{\gamma}} \right) \begin{pmatrix} \dot{\gamma}_{rr} \\ \dot{\gamma}_{r\theta} \end{pmatrix}, \quad (2.7)$$

$$\dot{\gamma}_{rr} = 2 \frac{\partial u}{\partial r}, \quad \dot{\gamma}_{r\theta} = \frac{1}{r} \frac{\partial u}{\partial \theta} + \frac{\partial v}{\partial r} - \frac{v}{r}, \tag{2.8a,b}$$

$$\dot{\gamma} = \sqrt{\left(\frac{1}{r} \frac{\partial u}{\partial \theta} + \frac{\partial v}{\partial r} - \frac{v}{r}\right)^2 + 4 \left(\frac{\partial u}{\partial r}\right)^2}. \tag{2.9}$$

The boundary conditions are

$$(u, v) = (0, 0) \quad \text{at } \theta = \pm\alpha, \tag{2.10}$$

$$v = \frac{\partial u}{\partial \theta} = 0 \quad \text{at } \theta = 0, \tag{2.11}$$

which express no slip at the edges of the wedge (2.10) and symmetry about the mid-line (2.11). There is, additionally, an integral expression for the volume flux per unit width given by

$$\int_{-\alpha}^{\alpha} ru \, d\theta = -1. \tag{2.12}$$

The residual dimensionless parameter is given by

$$Bi = \frac{R^2 \tau_c}{\mu Q}, \tag{2.13}$$

which defines a Bingham number, giving the ratio of plastic to viscous stresses. Note that this Bingham number depends on the scale of the radial distance from the vertex, due to the geometry imposing no other length scale. For given rheological parameters and volume flux, the parameters define a critical dimensional radial distance, $r_c = (\mu Q / \tau_c)^{-1/2}$, below which viscous forces dominate, and beyond which plastic forces dominate the flow. We will concern ourselves with the $Bi \gg 1$ (plastically dominated) and $Bi \ll 1$ (viscously dominated) regimes, which apply sufficiently far from and sufficiently close to the vertex, respectively. We note that we could have chosen to scale radial distances by r_c , in which case all dimensional parameters are removed from the governing equation. However, our exposition is clearer and easier to compare with previous studies when based upon the dimensionless variables and governing equations given above. We note that, due to the quadratic dependence of Bi on R , we anticipate that our asymptotic expansions will be functions of $r^2 Bi$. The absence of inertial terms in (2.4)–(2.6) requires that the Reynolds number, $Re = \rho Q / \mu$, is sufficiently small. In practice this requirement varies depending on the regime of interest. For the $Bi \gg 1$ regime it will be sufficient that $Re = O(1)$, while for the $Bi \ll 1$ regime we will require $Re \ll Bi$.

2.1. An outline of the solution

Before performing a detailed analysis of the problem, we outline the key results. In this discussion we assume that the wedge extends from a large dimensional radius, $r \gg r_c$, to a small radius $r \ll r_c$. Thus, in the far field of the wedge, and away from the walls, the leading-order flow is given by Nadai’s solution for converging plastic flow (Nadai 1924; Hill 1950),

$$u = -\frac{A}{r(c - \cos 2\psi)}, \quad v = 0, \quad \frac{d\psi}{d\theta} = c \sec 2\psi - 1. \tag{2.14a-c}$$

Here, A and c are constants determined by the flux and boundary conditions, respectively, which are given explicitly later in (3.14) and (3.15). The function ψ measures the angle

The converging flow of viscoplastic fluid

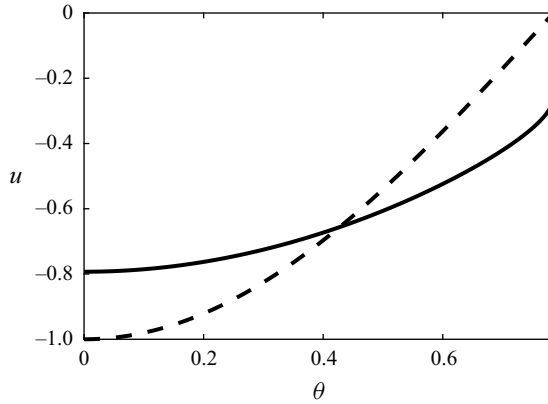


Figure 2. The radial velocity field, u , as a function of polar angle, θ , for plastic (solid line) and viscous (dashed line) converging flow in a wedge, with $\alpha = \pi/4$ and $r = 1$ (see (2.14a–c) and (2.15a–c)).

between the directions of the principle stresses and the coordinate axes, and is a function of the polar angle, such that $\tau_{r\theta} = \tau_{rr} \tan 2\psi$. Viscous shear-stress-dominated flow will be shown to be confined to a thin boundary layer of angular thickness $O((r^2 Bi)^{-1/2})$, allowing the solution to satisfy no slip. The variation of the angular extent of the boundary layer with r is such that the boundary layer is of a constant Cartesian thickness along the no-slip boundary. The first-order corrections to the plastic flow (2.14a–c) will be shown to also be $O((r^2 Bi)^{-1/2})$ and are driven by the flow within the boundary layer. A thin intermediate layer is also required between the bulk of the wedge and the boundary layer, for asymptotic matching of the respective solutions in these regions. One interpretation of this boundary layer structure is that the plastically dominated bulk solution, (2.14a–c), suffers from two different inconsistencies at the wall, namely diverging shear rates and slip, which require addressing at different scales. The intermediate layer plays the role of regularising the divergent shear rates, while the boundary layer enforces the no-slip boundary condition.

In contrast, at the outflow of the wedge, the shear rate is much higher due to radial convergence, and viscous forces dominate the flow. The leading-order flow is the classical Stokes solution,

$$u = -\frac{\cos(2\theta) - \cos(2\alpha)}{r(\sin(2\alpha) - 2\alpha \cos(2\alpha))}, \quad v = 0, \quad p = -\frac{2 \cos 2\theta}{r^2(\sin 2\alpha - 2\alpha \cos 2\alpha)} + \text{const.}, \quad (2.15a-c)$$

which defines a purely converging flow for all $\alpha \leq \pi/2$. Here, the first-order corrections due to plasticity are $O(r^2 Bi)$. Comparison of the radial velocity profiles in the plastic and viscous limits (figure 2), shows that the viscous profile has enhanced flow at the centre of the wedge compared to the plastic flow. A consequence of this is that we expect an angular velocity to be induced towards the centre of the wedge, away from the walls, to satisfy conservation of mass as the fluid transitions from the plastic profile at the inflow to the viscous profile at the outflow. This is indeed borne out and quantified in the analytical solution constructed below.

3. Plastic regime ($Bi \gg 1$)

In the regime of large Bingham number, $Bi \gg 1$, or equivalently at large distances from the apparent apex of the wedge, the constitutive equation (2.7) has three main regimes for

different sizes of the strain rate, $\dot{\gamma}$: plastic stresses dominate the momentum balance when the strain rate is $O(1)$; viscous stresses dominate in a thin boundary layer where the strain rate is high; and both become significant for an intermediate magnitude of the strain rate.

3.1. *The bulk solution*

In the bulk of the wedge, away from the boundaries, we expect that $\dot{\gamma} = O(1)$. In this case the constitutive equation is dominated by the yield stress and we find that the deviatoric stresses are determined up to $O(1)$ by the plastic flow equation

$$\tau_{ij} = Bi \frac{\dot{\gamma}_{ij}}{\dot{\gamma}}, \tag{3.1}$$

which implies that, at leading order, the magnitude of the deviatoric stress is everywhere equal to the yield stress, and that the deviatoric stress aligns with the rate of strain. As for the flow in an eccentric annulus (Walton & Bittleston 1991) and gravitationally driven shallow layer flow (Balmforth & Craster 1999), while the stress does not exceed the yield stress at leading order, the material is nonetheless undergoing deformation, and so must be yielded. This region is therefore analogous to ‘pseudo-plugs’ found in other flow scenarios (Walton & Bittleston 1991; Balmforth & Craster 1999).

Following the approach of Nadai (1924) in the bulk of the flow we introduce a variable, ψ , such that

$$\begin{pmatrix} \tau_{rr} \\ \tau_{r\theta} \end{pmatrix} = Bi \begin{pmatrix} \cos 2\psi \\ \sin 2\psi \end{pmatrix}. \tag{3.2}$$

We must have $\psi(r, 0) = 0$ by symmetry, and in the analysis that follows will focus on the region $0 \leq \theta \leq \alpha$, with symmetry allowing the automatic construction of the flow in $-\alpha \leq \theta \leq 0$. In the solution of Nadai (1924), (2.14a–c), the velocity does not vanish on the wall. Hence, to satisfy the no-slip boundary condition, we expect the shear rate, $\partial u / \partial \theta$, to become large in a small region near the walls. This leads to a different regime where the viscous stresses are no longer negligible in the balance of momentum. We define the angle, θ_Y , at which this change of dynamical balance occurs by

$$\theta_Y = \alpha - \epsilon \Phi(r), \tag{3.3}$$

where ϵ is a small parameter depending on Bi in a way that is yet to be determined, and we have introduced a potential dependence on r through the function Φ . The notation θ_Y alludes to the fact that this is a fake yield surface, delineating weakly yielded fluid from highly sheared, fully yielded fluid adjacent to the boundary.

The governing equation (3.2) can be rearranged to obtain

$$\tan(2\psi) = \frac{\tau_{r\theta}}{\tau_{rr}} = \frac{\dot{\gamma}_{r\theta}}{\dot{\gamma}_{rr}}. \tag{3.4}$$

At the wall, $\dot{\gamma}_{rr}$ vanishes, and in the thin boundary layer, $\dot{\gamma}_{r\theta}$ is large. Hence, both ratios on the right-hand side of (3.4) are large in the boundary layer, and we require $\psi \rightarrow \pi/4$ as $\theta \rightarrow \theta_Y$ in order for the bulk solution to match to the boundary layer. This dependence of ψ on r through the boundary condition at $\theta = \pm\theta_Y(r)$, leads to apparent difficulties in the asymptotic investigation of the boundary layer due to divergent strain rates which obfuscate the straightforward expansion of the flow variables. To avoid this difficulty, we use strained coordinates, introducing a coordinate transform that transforms the fake yield

The converging flow of viscoplastic fluid

surfaces, $\theta = \pm\theta_Y(r)$, to $\Theta = \pm 1$. Specifically we make the transformation of independent variables

$$(r, \theta) = (r, \theta_Y(r)\Theta), \tag{3.5}$$

noting that this gives partial derivatives:

$$\frac{\partial}{\partial r} \rightarrow \frac{\partial}{\partial r} + \frac{\partial\Theta}{\partial r} \frac{\partial}{\partial\Theta} = \frac{\partial}{\partial r} + \frac{\epsilon\Phi'\Theta}{\alpha - \epsilon\Phi} \frac{\partial}{\partial\Theta}, \quad \frac{\partial}{\partial\theta} \rightarrow \frac{\partial\Theta}{\partial\theta} \frac{\partial}{\partial\Theta} = \frac{1}{\alpha - \epsilon\Phi} \frac{\partial}{\partial\Theta}. \tag{3.6a,b}$$

In the plastically dominated region we seek a solution that is, to leading order, radial. The boundary layer may drive an azimuthal flow of order ϵ , so we search for a solution of the form

$$u = u_0 + \epsilon u_1 + \dots, \quad v = \epsilon v_1 + \dots, \quad \psi = \psi_0 + \epsilon \psi_1 + \dots, \quad p = p_0 + \epsilon p_1 + \dots \tag{3.7a-d}$$

We have three governing equations. The curl of the momentum balance gives

$$\left(\frac{1}{(\alpha - \epsilon\Phi)^2} \frac{\partial^2}{\partial\Theta^2} - \left(r \frac{\partial}{\partial r} + \frac{\epsilon r\Phi'\Theta}{\alpha - \epsilon\Phi} \frac{\partial}{\partial\Theta} \right)^2 - 2 \left(r \frac{\partial}{\partial r} + \frac{\epsilon r\Phi'\Theta}{\alpha - \epsilon\Phi} \frac{\partial}{\partial\Theta} \right) \right) \sin 2\psi + \frac{2}{\alpha - \epsilon\Phi} \frac{\partial}{\partial\Theta} \left(r \frac{\partial}{\partial r} + \frac{\epsilon r\Phi'\Theta}{\alpha - \epsilon\Phi} \frac{\partial}{\partial\Theta} + 1 \right) \cos 2\psi = 0; \tag{3.8}$$

conservation of mass gives

$$\left(\frac{\partial}{\partial r} + \frac{\epsilon\Phi'\Theta}{\alpha - \epsilon\Phi} \frac{\partial}{\partial\Theta} \right) (ru) + \frac{1}{\alpha - \epsilon\Phi} \frac{\partial v}{\partial\Theta} = 0; \tag{3.9}$$

and, provided we remain above $O(Bi^{-1})$ in (3.7a-d), at which point viscous terms re-enter the constitutive equation, the rigid plastic approximation holds and the orientation of the stress tensor, parameterised through ψ (3.2), is given by

$$2 \tan 2\psi \left(r \frac{\partial u}{\partial r} + \frac{\epsilon r\Phi'\Theta}{\alpha - \epsilon\Phi} \frac{\partial u}{\partial\Theta} \right) = \frac{1}{\alpha - \epsilon\Phi} \frac{\partial u}{\partial\Theta} + r \frac{\partial v}{\partial r} + \frac{\epsilon r\Phi'\Theta}{\alpha - \epsilon\Phi} \frac{\partial v}{\partial\Theta} - v. \tag{3.10}$$

3.2. Leading-order bulk flow

At $O(1)$ the solution of (3.8)–(3.10) corresponds to Nadai’s (1924) solution up to the slight alteration of the factors of α due to the scaling to unit angle. Specifically, we have

$$\alpha\Theta = -\psi_0 + \frac{c}{\sqrt{c^2 - 1}} \arctan \left(\sqrt{\frac{c+1}{c-1}} \tan \psi_0 \right), \tag{3.11}$$

$$u_0 = -\frac{A}{r(c - \cos(2\psi_0))}, \tag{3.12}$$

$$p_0 = 2Bic \ln(r) + Bic \ln(c - \cos 2\psi_0) + \text{const.} \tag{3.13}$$

The constant, c , is determined by the boundary condition $\psi_0(1) = \pi/4$, as required to match to a shear-stress-dominated boundary layer (see discussion after (3.4)). This gives

the implicit equation

$$\alpha + \frac{\pi}{4} = \frac{c}{\sqrt{c^2 - 1}} \arctan \left(\sqrt{\frac{c+1}{c-1}} \right). \quad (3.14)$$

Finally, A is determined by the volume-flux condition. To leading order,

$$A = \frac{2c(c^2 - 1)}{4\alpha + \pi + 2c}. \quad (3.15)$$

3.3. *The intermediate layer*

Asymptotic analysis of this leading-order solution (see [Appendix A](#)) verifies that the shear rate diverges as we approach the fake yield surface, $\theta = \theta_Y$, thus we will require an intermediate layer around $\Theta = 1$, to regularise the diverging terms. We proceed following [Walton & Bittleston \(1991\)](#) and [Balmforth & Craster \(1999\)](#), to derive a governing equation that reduces to the appropriate dynamical balances as we move out of the intermediate layer into either the bulk or boundary layer regions. We define this intermediate layer by the further coordinate transformation $\delta\zeta = \theta_Y - \theta = (\alpha - \epsilon\Phi)(1 - \Theta)$, where ζ is our new angular coordinate and δ is another ordering parameter. We re-label velocity components

$$\begin{pmatrix} u \\ v \end{pmatrix} = \begin{pmatrix} U \\ \epsilon V \end{pmatrix}, \quad (3.16)$$

where U and V are assumed to be $O(1)$. It is assumed, and later verified, that $\delta \ll \epsilon \ll 1$, so that the intermediate layer is much narrower than both the bulk region and the boundary layer. The ϵ scaling of the azimuthal velocity is inherited from the bulk solution ([3.7a–d](#)).

Note that,

$$\delta\zeta = \alpha - \epsilon\Phi(r) - \theta, \quad (3.17)$$

and so, as before, we have altered partial derivatives

$$\frac{\partial}{\partial r} \rightarrow \frac{\partial}{\partial r} - \frac{\epsilon\Phi'}{\delta} \frac{\partial}{\partial \zeta}, \quad \frac{\partial}{\partial \theta} \rightarrow -\frac{1}{\delta} \frac{\partial}{\partial \zeta}. \quad (3.18a,b)$$

Expansion of the leading-order plastic solution for small δ (see [Appendix A](#)), gives

$$u_0 = -\frac{A}{rc} - \frac{2A}{rc\sqrt{c}}\sqrt{\delta\zeta} + \dots, \quad (3.19)$$

thus we define

$$U = U_0(r) + \delta^{1/2}U_1(r, \zeta) + \dots, \quad \text{with } U_0(r) = -\frac{A}{cr}, \quad (3.20)$$

and the term $U_1(r, \zeta)$ capturing the weak variation of U with ζ over the width of the intermediate layer. In addition to the assumption that $\delta \ll \epsilon \ll 1$, we will now also work under the assumption that $\epsilon^2 \ll \delta$ which ensures that the additional terms from the coordinate transformation do not enter the leading-order balance, and is also required for the second term in [\(3.19\)](#) to be greater than contributions to the velocity from the order- ϵ correction terms in the bulk solution.

The converging flow of viscoplastic fluid

Under this assumption, verified below, expanding the shear stress gives

$$\tau_{r\theta} = -\frac{1}{r}\delta^{-1/2}\partial_\zeta U_1 + Bi - 2r^2\delta Bi \left(\frac{\partial_r U_0}{\partial_\zeta U_1}\right)^2 + \dots, \quad (3.21)$$

where we now use short-hand notation for partial derivatives for notational clarity. The second term on the right-hand side of (3.21) is constant and so does not contribute to the momentum balance, hence we have both viscous and plastic terms when $\delta = Bi^{-2/3}$. The leading-order radial and angular expressions of momentum balance are now given by

$$Bi^{-1}\partial_r p = \frac{1}{r^2}\partial_\zeta \partial_\zeta U_1 + 2r\partial_\zeta \left[\left(\frac{\partial_r U_0}{\partial_\zeta U_1}\right)^2\right], \quad (3.22)$$

$$Bi^{-1/3}\partial_\zeta p = 2r\partial_\zeta \left[\frac{\partial_r U_0}{\partial_\zeta U_1}\right], \quad (3.23)$$

which, along with the fact that p is $O(Bi)$ from the bulk solution, imply $p = Bi P(r) = 2cBi \ln r$ to leading order. Thus, the radial pressure gradient is unchanged to leading order by the intermediate layer.

The asymptotic behaviour of the shear stress in the bulk solution is given by

$$\tau_{r\theta} = Bi \sin 2\psi_0 = Bi - 2cBi\delta\zeta + \dots = Bi - 2cBi^{1/3}\zeta\dots, \quad (3.24)$$

(see Appendix A). Then, integrating (3.22) once with respect to ζ and using (3.24) and (3.21) at $O(Bi^{1/3})$ to set the constant of integration, we establish a cubic equation in $\partial_\zeta U_1$,

$$(\partial_\zeta U_1)^3 - r^2\zeta\partial_r P(\partial_\zeta U_1)^2 + 2r^3(\partial_r U_0)^2 = 0, \quad (3.25)$$

in the intermediate layer. Substituting for $U_0(r)$ and $P(r)$, we find the form

$$(\partial_\zeta U_1)^3 - 2cr\zeta(\partial_\zeta U_1)^2 + \frac{2A^2}{c^2r} = 0. \quad (3.26)$$

For the angular component of the velocity, from the incompressibility equation we have

$$\frac{\partial}{\partial r}(rU) - \frac{\epsilon r\Phi'}{\delta}\frac{\partial U}{\partial \zeta} - \frac{\epsilon}{\delta}\frac{\partial V}{\partial \zeta} = 0, \quad (3.27)$$

which, on substitution of (3.20), leads to

$$V = V_0(r) - \delta^{1/2}r\Phi'U_1(r, \zeta) + \dots \quad (3.28)$$

It remains to find V_0 and Φ by solving in the boundary layer (§ 3.4).

We deduce some matching information for the boundary layer by considering the behaviour of the cubic equation for $\partial_\zeta U_1$, (3.26). As $\zeta \rightarrow -\infty$, in (3.26), the diverging positive second term can only balance with the first term, and so $\partial_\zeta U_1 \rightarrow -\infty$ and we have

$$\partial_\zeta U_1 \sim 2cr\zeta. \quad (3.29)$$

Hence, as we move into the boundary layer, we integrate (3.29) to find the velocity profile satisfies

$$U = U_0(r) + crBi^{-1/3}\zeta^2 + Bi^{-1/3}W(r) + \dots, \quad (3.30)$$

where $W(r)$ is an arbitrary function of integration. Immediately, we identify the new distinguished scaling as $Bi^{-1/3}\zeta^2 = O(1)$, or $\zeta = O(Bi^{1/6})$ which, when related back in terms of θ , gives $\theta - \theta_Y = O(Bi^{-1/2})$. Thus we have derived the width of the boundary layer as $\epsilon = Bi^{-1/2}$, and can verify that $\epsilon^2 = Bi^{-1} \ll \delta \ll \epsilon$, as was assumed in deriving the leading order stress balance in the intermediate layer above.

3.4. *Boundary layer solution*

The boundary layer solution is constructed by introducing the scaled coordinate, $\epsilon\tilde{\phi} = \alpha - \theta$. From mass conservation we find the natural scalings

$$\begin{pmatrix} u \\ v \end{pmatrix} = \begin{pmatrix} \tilde{U} \\ \epsilon\tilde{V} \end{pmatrix}, \tag{3.31}$$

where \tilde{U} and \tilde{V} are assumed $O(1)$. Then, expanding the shear stress gives

$$\tau_{r\theta} = -\frac{1}{\epsilon r} \frac{\partial \tilde{U}}{\partial \tilde{\phi}} + Bi + O(\epsilon^2 Bi), \tag{3.32}$$

where the sign of the Bi term on the right-hand side arises due to $\partial \tilde{U} / \partial \tilde{\phi} < 0$ (since U varies from 0, at the wall, to some negative value in the bulk of the flow). Thus, viscous stresses balance the pressure gradient since $\epsilon^3 Bi = Bi^{-1/2} \ll 1$ and so the plastic shear-stress terms are omitted in the radial momentum balance. We find that, as in the intermediate layer, the pressure is constant across the extent of the boundary layer to leading order, and is thus set by the pressure in the bulk and intermediate regions. The radial momentum equation then becomes

$$\frac{\partial P}{\partial r} \equiv \frac{2c}{r} = \frac{1}{r^2} \frac{\partial^2 \tilde{U}}{\partial \tilde{\phi}^2}, \tag{3.33}$$

which integrates to give

$$\tilde{U} = cr(\tilde{\phi}^2 - 2\Phi(r)\tilde{\phi}). \tag{3.34}$$

The constants of integration have been chosen so that $\partial \tilde{U} / \partial \tilde{\phi} = 0$ at $\tilde{\phi} = \Phi$, and $\tilde{U} = 0$ at $\tilde{\phi} = 0$.

As $\tilde{\phi} \rightarrow \Phi$ we may write

$$\tilde{U} = -cr\Phi^2 + cr(\tilde{\phi} - \Phi)^2, \tag{3.35}$$

which is consistent with the $\zeta \rightarrow -\infty$ limit, (3.30), and, from (3.20), determines Φ ,

$$\Phi(r) = \frac{\sqrt{A}}{cr}. \tag{3.36}$$

Thus we have found that the angular width of the boundary layer, $\epsilon\Phi$, does indeed depend on $(r^2 Bi)^{-1/2}$, as anticipated. The Cartesian width of this boundary layer is $\epsilon r \Phi = Bi^{-1/2} \sqrt{A}/c$. It is therefore a constant, independent of the radial distance from the apex of the wedge. We can also now calculate the additional shear stress at the wall due to the viscoplastic boundary layer. From (3.32) we have

$$\tau_{r\theta}|_{\theta=\alpha} = Bi - \frac{1}{\epsilon r} \frac{\partial \tilde{U}}{\partial \tilde{\phi}} \Big|_{\tilde{\phi}=0} + \dots = Bi + \sqrt{Bi} \frac{2\sqrt{A}}{r} + \dots, \tag{3.37}$$

demonstrating that the additional shear stress at the wall is $O(Bi^{1/2})$ and is proportional to $1/r$. Thus, the additional shear force over the extent of the upper wall, from $r = r_1$ to

$r = r_2$, assuming the plastic regime applies throughout this domain, is given by

$$2\sqrt{Bi}\sqrt{A} \ln\left(\frac{r_2}{r_1}\right). \tag{3.38}$$

For the polar velocity, using incompressibility, we have

$$\frac{\partial \tilde{V}}{\partial \tilde{\phi}} = -\frac{1}{\epsilon} \frac{\partial \tilde{V}}{\partial \theta} = -\frac{\partial v}{\partial \theta} = \frac{\partial}{\partial r}(r\tilde{U}) = 2cr\tilde{\phi}^2 - 2\sqrt{A}\tilde{\phi}. \tag{3.39}$$

Integrating and using $\tilde{V} = 0$ at $\tilde{\phi} = 0$, yields

$$\tilde{V} = \frac{cr}{3}(2\tilde{\phi}^3 - 3\tilde{\phi}^2). \tag{3.40}$$

In particular, by matching \tilde{V} to V_0 (see (3.28)), we find the negative angular flow,

$$V_0(r) = -\frac{cr\Phi^3}{3} = -\frac{A\sqrt{A}}{3c^2r^2}. \tag{3.41}$$

This velocity away from the boundary is transmitted through the intermediate layer to the bulk region. To determine the profile of this weak angular flow in the body of the wedge requires exploring higher orders in the bulk solution. This is done in § 3.5.

It is interesting to consider the limit $\alpha \rightarrow 0$ with $r\alpha = 1$, for which $A/c^2 \rightarrow 1$. In this limit: the leading-order bulk solution reduces to a uniform plug flow; the intermediate layer vanishes; the leading-order solution in the uniform width, $O(Bi^{-1/2})$, boundary layer becomes a parabolic profile; and the outflow from the boundary layer, ϵV_0 , vanishes. Thus the Bingham–Poiseuille flow in a channel is recovered, as it must be, in this limit.

3.5. Higher orders in the bulk

At $O(\epsilon)$, the governing system of equations (3.8)–(3.10) becomes

$$\begin{aligned} &\left(\frac{1}{\alpha^2} \frac{\partial^2}{\partial \Theta^2} - \left(r \frac{\partial}{\partial r}\right)^2 - 2r \frac{\partial}{\partial r}\right) (\psi_1 \cos 2\psi_0) - \frac{2}{\alpha} \frac{\partial}{\partial \Theta} \left(r \frac{\partial}{\partial r} + 1\right) (\psi_1 \sin 2\psi_0) \\ &= -\left(\frac{\Phi}{\alpha^3} \frac{\partial^2}{\partial \Theta^2} + \frac{\Phi \Theta}{2\alpha} \frac{\partial}{\partial \Theta}\right) \sin 2\psi_0 + \frac{\Phi \Theta}{\alpha^2} \frac{\partial^2}{\partial \Theta^2} \cos 2\psi_0, \end{aligned} \tag{3.42}$$

$$\frac{\partial (ru_1)}{\partial r} + \frac{1}{\alpha} \frac{\partial v_1}{\partial \Theta} = \frac{\Phi \Theta}{\alpha} \frac{\partial u_0}{\partial \Theta}, \tag{3.43}$$

$$\begin{aligned} &2r \tan 2\psi_0 \frac{\partial u_1}{\partial r} - \frac{1}{\alpha} \frac{\partial u_1}{\partial \Theta} - r \frac{\partial v_1}{\partial r} + v_1 - 4\psi_1 u_0 \sec^2 2\psi_0 \\ &= 2 \frac{\Phi \Theta}{\alpha} \tan 2\psi_0 \frac{\partial u_0}{\partial \Theta} + \frac{\Phi}{\alpha^2} \frac{\partial u_0}{\partial \Theta}, \end{aligned} \tag{3.44}$$

where the identities, $r(d\Phi/dr) = -\Phi$ and $r(\partial u_0/\partial r) = -u_0$, have been used. The right-hand sides of (3.42)–(3.44) determine the r dependence of u_1 , v_1 and ψ_1 , and so

we define

$$u_1 = \frac{\hat{u}_1(\Theta)}{r^2}, \quad v_1 = \frac{\hat{v}_1(\Theta)}{r^2}, \quad \text{and} \quad \psi_1 = \frac{\hat{\psi}_1(\Theta)}{r}. \quad (3.45a-c)$$

Making these substitutions, along with $\Phi = \sqrt{A}/cr$, results in the coupled ordinary differential equations (ODEs)

$$\begin{aligned} & \frac{1}{\alpha^2}(\hat{\psi}_1 \cos 2\psi_0)'' + \hat{\psi}_1 \cos 2\psi_0 \\ &= \frac{\sqrt{A}}{\alpha c} \left(\frac{\Theta}{\alpha} (\cos 2\psi_0)'' - \frac{1}{\alpha^2} (\sin 2\psi_0)'' - \frac{\Theta}{2} (\sin 2\psi_0)' \right), \end{aligned} \quad (3.46)$$

$$-\hat{u}_1 + \frac{1}{\alpha} \hat{v}'_1 = \frac{\sqrt{A}\Theta}{\alpha c} \hat{u}'_0, \quad (3.47)$$

$$-4\hat{u}_1 \tan 2\psi_0 - \frac{1}{\alpha} \hat{u}'_1 + 3\hat{v}_1 - 4\hat{\psi}_1 \hat{u}_0 \sec^2 2\psi_0 = \frac{\sqrt{A}}{\alpha c} \left(2\Theta \tan 2\psi_0 + \frac{1}{\alpha} \right) \hat{u}'_0. \quad (3.48)$$

There are two boundary conditions for $\hat{v}_1(\Theta)$

$$\hat{v}_1(0) = 0, \quad \hat{v}_1(1) = -\frac{A\sqrt{A}}{3c^2}, \quad (3.49a,b)$$

which respectively represent the symmetry of the flow at the mid-line and matching to the angular outflow from the boundary layer. Additionally, the symmetry conditions demand that

$$\hat{\psi}_1(0) = 0. \quad (3.50)$$

The final boundary condition arises from matching the deviatoric stresses between the intermediate layer and the bulk solution. Specifically, in the intermediate layer, using the transformed partial derivatives, (3.18a,b), the asymptotic form of the radial velocity, (3.20), and the identity $r\Phi' = -\Phi$, we have (in the notation of the intermediate layer)

$$\tau_{rr} = -\frac{2rBi \delta^{1/2}}{\partial_\zeta U_1} \left(\frac{dU_0}{dr} - \frac{\epsilon}{\delta^{1/2}} \Phi' \partial_\zeta U_1 \right) + \dots = \frac{2U_0}{\partial_\zeta U_1} Bi^{2/3} - 2\Phi Bi^{1/2} + \dots \quad (3.51)$$

By considering the $\zeta \rightarrow \infty$ limit of the cubic (3.26), we find that $\partial_\zeta U_1 \rightarrow -A/(r\sqrt{c^3\zeta})$, and so

$$\tau_{rr} = 2\sqrt{c\zeta} Bi^{2/3} - 2\Phi Bi^{1/2} + \dots \quad (3.52)$$

Meanwhile, in the bulk solution, we have

$$\tau_{rr} = Bi \cos 2\psi_0 - 2\epsilon Bi \psi_1 \sin 2\psi_0 + \dots = 2Bi\sqrt{\alpha c(1-\Theta)} - 2Bi^{1/2}\psi_1 + \dots, \quad (3.53)$$

where we have used the expansion of $\cos 2\psi_0$ and $\sin 2\psi_0$ about $\Theta = 1$, given in Appendix A. Finally, using the substitution $\delta\zeta = \theta_Y(1-\Theta) = \alpha(1-\Theta) + O(\epsilon\delta)$, we see that the leading-order terms match, and that matching at $O(Bi^{1/2})$ requires

$$\psi_1(r, \Theta = 1) = \Phi(r) = \frac{\sqrt{A}}{cr} \implies \hat{\psi}_1(1) = \frac{\sqrt{A}}{c}. \quad (3.54)$$

Furthermore, we may determine the behaviour of all the dependent variables in the regime $|1-\Theta| \ll 1$ (see Appendix B, setting $N = 1$ for the Bingham model).

The converging flow of viscoplastic fluid

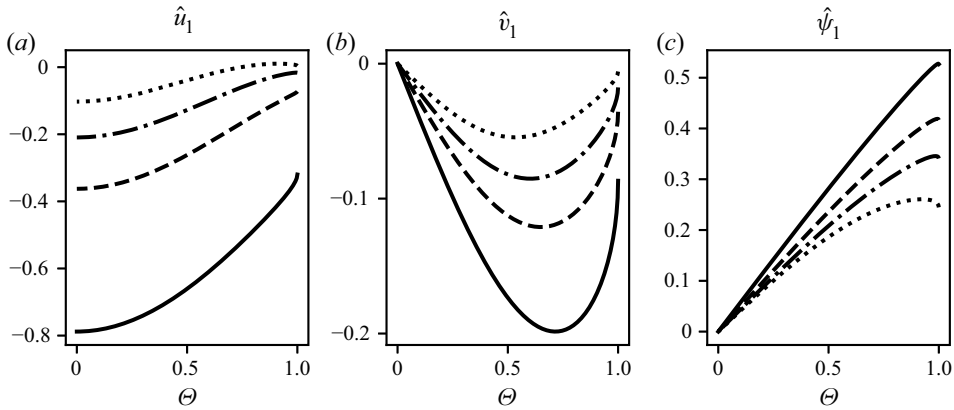


Figure 3. The first-order corrections to the velocities, u and v , and the stress orientation function, ψ , in the plastic regime, as functions of the scaled angular coordinate Θ , for $\alpha = \pi/6$ (solid), $\pi/4$ (dashed), $\pi/3$ (dash-dotted) and $\pi/2$ (dotted).

The boundary-value problem (3.46)–(3.48) was solved using a shooting method. First we use the local form of the dependent variables (B6)–(B8) to step a small distance, d , away from the singular point before integrating to $\Theta = 0$ where the boundary conditions (3.49a,b) and (3.50) determine the unknown coefficients, E and F , in (B6)–(B8). The dependence of the solutions on d was investigated and it was found that profiles were essentially independent of d for $d < 10^{-5}$. Numerical solutions are plotted for a range of values of α in figure 3. We note that the radial velocity is enhanced by the effects of the boundary layer, and that an angular velocity away from the boundary is induced, which reaches a maximum at some interior location. Also, the magnitude of the shear stress is promoted throughout the domain. The magnitude of these corrections decreases systematically with increasing wedge half-angle.

Physically, as we deviate from a perfectly rigid plastic, the radial flow is reduced by no slip at the wall, over an increasingly thick boundary layer. Thus, for the same volume flux, the radial flow must be enhanced in the centre of the wedge, and conservation of mass requires an angular flow from the wall, where radial flow is small, towards the centre of the wedge, where the flow is enhanced. The dependence on half-angle arises via the decreasing boundary layer strength with increasing half-angle. This occurs through a competition between the radial pressure gradient at the edge of the boundary layer (which decreases with increasing α , supporting a lower angular gradient of the shear stress potentially widening the boundary layer) and the magnitude of the non-vanishing velocity at the boundary in Nadai's (1924) plastic solution (2.14a–c) (which decreases with α , thus requiring a thinner boundary layer to enforce no slip for the same radial pressure gradient).

The balance between these effects is reflected in the \sqrt{A}/c factor in the boundary layer width, $\epsilon\Phi$. This term turns out to be a decreasing function of α , and so the boundary layer and the induced velocity perturbations are weaker for larger half-angles (at the same radial position, r). The stress behaviour is also non-trivial since the enhanced radial flow has the potential to increase both the normal radial stress, and the shear stress, but cannot increase both, since the magnitude of the deviatoric stress is everywhere equal to the yield stress at this order. However, as we have enhanced shear stress at the walls due to the viscoplastic shear layer, it is natural to expect the shear stress to be enhanced across the domain, as is observed.

3.6. Composite solutions

To produce leading-order radial and angular velocity profiles, it is useful to define a composite solution that is valid across the whole domain. We define such a solution, using the limiting behaviours of the plastic and boundary layer solutions in the vicinity of θ_Y , as

$$u_{comp}(r, \theta) = \begin{cases} u_0 + U + \frac{A}{rc} + \frac{2A\sqrt{\theta_Y - \theta}}{rc\sqrt{c}} & \text{for } \theta < \theta_Y, \\ \tilde{U} + U + \frac{A}{rc} - rcBi(\theta - \theta_Y)^2 & \text{for } \theta \geq \theta_Y, \end{cases} \quad (3.55)$$

$$v_{comp}(r, \theta) = \begin{cases} \epsilon \left(v_1 + V + \frac{A\sqrt{A}}{3r^2c^2} + \frac{2A\sqrt{A}}{r^2c^2\sqrt{c}}\sqrt{\theta_Y - \theta} \right) & \text{for } \theta < \theta_Y, \\ \epsilon \left(\tilde{V} + V + \frac{A\sqrt{A}}{3r^2c^2} - \sqrt{ABi}(\theta - \theta_Y)^2 \right) & \text{for } \theta \geq \theta_Y, \end{cases} \quad (3.56)$$

where $\theta_Y(r)$ is the location of the fake yield surface defined by (3.3) and (3.36). These profiles (for fixed r) are continuous at $\theta = \theta_Y$, since the velocities here are equal to those for the intermediate layer solution at $\zeta = 0$, on both branches of the piece-wise definition.

3.7. Numerical simulations

Numerical simulations of the complete governing partial differential equations (2.4)–(2.6), were carried out using the finite element method as implemented by FEniCS (Logg, Mardal & Wells 2012; Alnæs *et al.* 2015). The domains were meshed with 60 000 triangular elements, with a higher concentration at the wall and near the outflow, where higher strain rates are expected. The fluid is yielded everywhere, so we do not expect the occurrence of plug regions and the associated singular Jacobian matrix of the discretised equations, when applying the Newton method. Nonetheless, the nonlinearity in the equations causes problems when trying to use Newton iterations to converge to the solution from an arbitrary initial state. We found that using an augmented-Lagrangian method, as described by Saramito (2016), resulted in slow convergence but could be used to produce an effective initial guess for the Newton method, allowing a subsequent fast convergence to a Newton residual of less than 10^{-8} . For the following results Bi has been set at 1, but the domains have a radial range of $r \in [0.01, 500]$, allowing the effective Bingham number, r^2Bi , to vary from 10^{-4} to 250 000, within a single simulation. The low value of this parameter at the outflow means the purely viscous radial solution (2.15a–c) is a good approximation to the velocity at the outflow, and is therefore imposed as a Dirichlet boundary condition here, while the large value at the inflow means the leading-order asymptotic viscoplastic solution is an appropriate boundary condition here.

Firstly, we confirm the predicted behaviour of the boundary layer thickness in the plastic regime. For a given radius, the boundary layer thickness was determined from the numerical radial flow profile by the angle at which

$$\frac{\partial u}{\partial \theta} = \left(2Bi \frac{A^2}{c^2 r} \right)^{1/3}, \quad (3.57)$$

which is the shear rate predicted at the centre of the matching region by setting $\zeta = 0$ in the equation (3.26). Figure 4 shows the measured boundary layer thickness alongside the predicted value, $\epsilon\Phi(r)$, with Φ given by (3.36), at a number of radial positions for

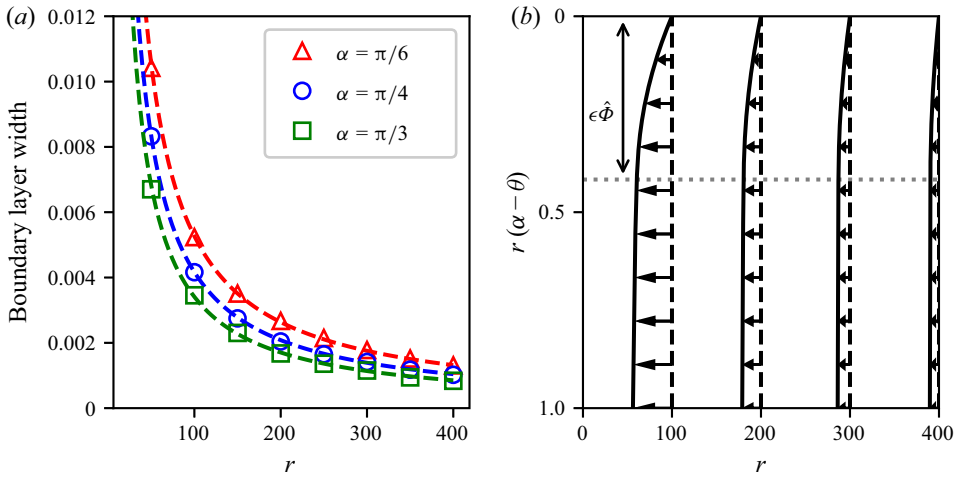


Figure 4. (a) The width of the viscoplastic boundary layer determined analytically (dashed) and numerically (symbols), at a range of radial positions and wedge angles. (b) Profiles of radial velocity determined numerically for $\alpha = \pi/4$. The quantity $r(\alpha - \theta)$ defines a small Cartesian distance from the wall at $\theta = \alpha$. The theoretical position of the fake yield surface is shown by a dotted line.

three different wedge angles, confirming the analytical result. Also shown are example velocity profiles from the numerical solution for $\alpha = \pi/4$, in a small region near the upper boundary $\theta = \alpha$. We note that the boundary layer is of constant width, in a Cartesian sense, due to the $1/r$ dependence of Φ , and that this is borne out by the numerical results.

Figure 5 provides comparisons between the numerical and composite asymptotic flow profiles for a choice of wedge angle ($\alpha = \pi/4$) and radius ($r = 100$), which is sufficiently distant from the inflow and outflow boundaries to exhibit the fully developed profile. The numerical simulations accurately reproduce the predicted velocity profiles in both the bulk and boundary layer regions. In particular, the predicted weak negative angular flow is confirmed in these simulations.

Finally, we note the small discrepancy in panel (b) of figure 5 and explore whether this can be explained by the absence of higher-order terms in the asymptotic expansions. This is confirmed by figure 6, which shows the difference between the leading-order composite solutions and the numerical solutions, measured by the L_2 -norm at fixed r

$$\Delta u(r) = \sqrt{\int_0^\alpha [u_{num}(r, \theta) - u_{comp}(r, \theta)]^2 d\theta}, \quad (3.58)$$

$$\Delta v(r) = \sqrt{\int_0^\alpha [v_{num}(r, \theta) - v_{comp}(r, \theta)]^2 d\theta}. \quad (3.59)$$

For the velocity in the radial direction, the composite solution neglects terms of $O(Bi^{-1/2})$, which results in Δu proportional to $Bi^{-1/2}r^{-2} = r^{-2}$ for fixed Bi . For the velocity in the angular direction we must consider the order of terms neglected above $O(Bi^{-1/2})$. From (3.30), we expect an $O(Bi^{-1/3})$ correction to the radial flow in the boundary layer. This in turn would drive a correction of $O(\epsilon Bi^{-1/3}) = Bi^{-5/6}$ in the velocity in the angular direction at the top of the boundary layer. Hence, without calculating higher orders explicitly, we expect the second-order correction to the velocity to be $O(Bi^{-5/6})$ or, including radial dependence, $O(r^{-8/3}Bi^{-5/6})$, since the expansion parameter is r^2Bi

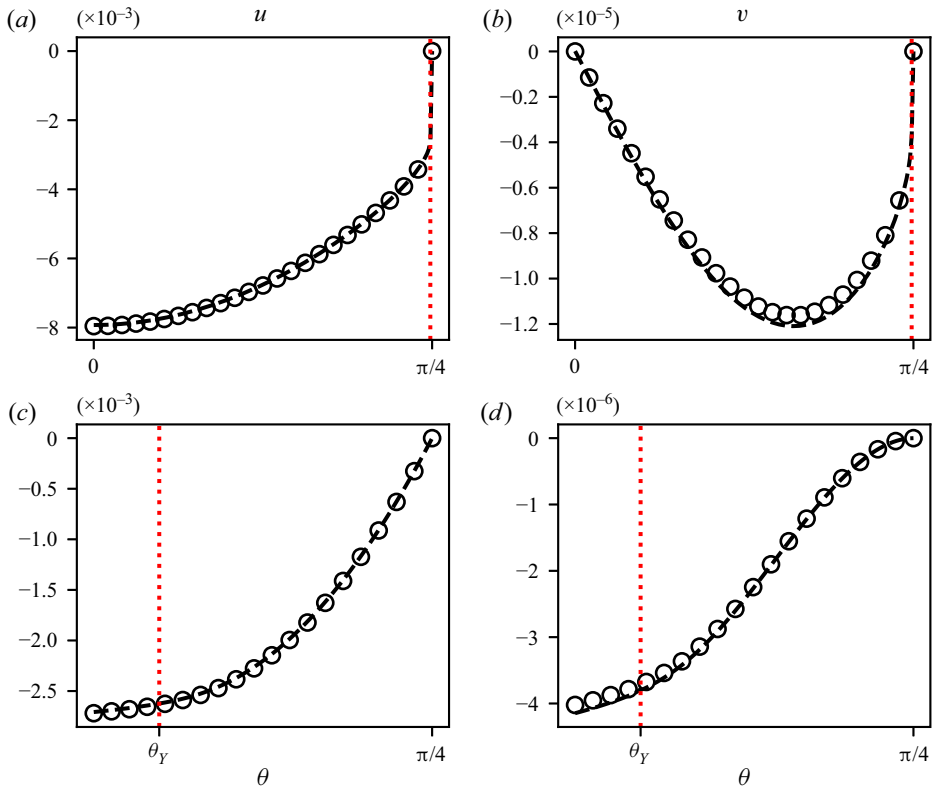


Figure 5. The asymptotic (dashed line) and numerical (circles) radial and angular velocities as function of angle, θ , for $\alpha = \pi/4$, $Bi = 1$ and $r = 100$. The numerical data points shown are only a small sub-sample of the full numerical solutions, which are of a much higher resolution. (a,b) Plot the radial and angular velocities respectively, across the domain. (c,d) Are close-ups of the boundary layers for (a,b) respectively. The position of the fake yield surface, θ_Y , is depicted by a red dotted line in all panels (and is almost indistinguishable from the boundary, $\theta = \pi/4$, in the upper two panels).

and the leading-order flow has r^{-1} dependence. Hence, we expect Δv to scale like $r^{-8/3}$. Figure 6 confirms this relationship for the three wedge angles studied, providing strong evidence for the validity of our asymptotic structure. The deviation from the predicted trends at $r \approx 500$ is due to the leading-order profiles being imposed here as boundary conditions, and so the difference is at the level of the implementation precision.

Figure 7 shows a density plot of log strain-rate and radial velocity profiles from the numerical solution for the wedge of half-angle $\alpha = \pi/3$. These demonstrate how the plastically dominated regime, with a thin boundary layer structure, is valid for large values of r , but transitions to a different regime, without a boundary layer, towards the apparent apex of the wedge. For sufficiently small values of r the viscous stresses are dominant and a new asymptotic solution can be derived. This is detailed in the next section.

4. The viscous regime

In the regime of small Bingham number, $Bi \ll 1$, or, equivalently, at small distances from the apex of the wedge, the viscoplastic problem is a regular perturbation of the viscous Stokes problem, and so we do not require a boundary layer structure. This regime has been studied previously by Sandru & Camenshi (1979), so we initially outline this solution

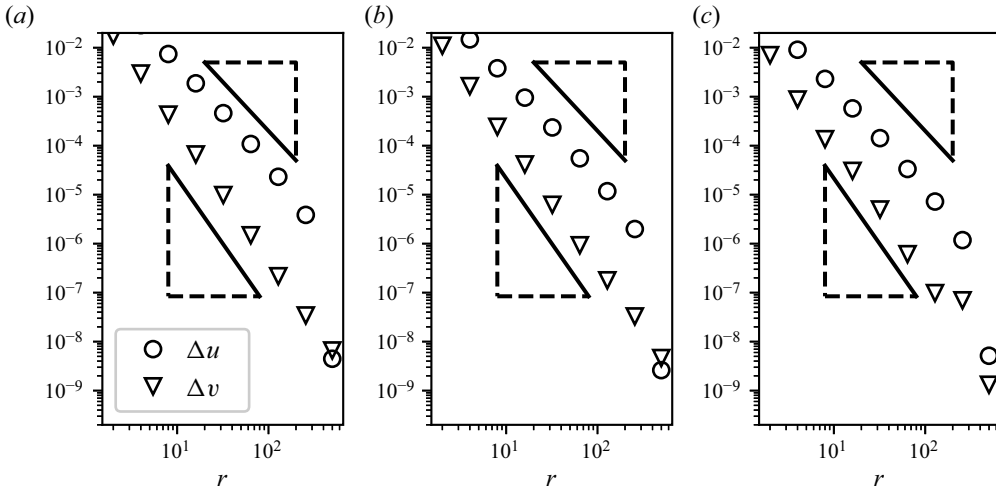


Figure 6. The difference between the leading-order asymptotic and numerical solutions for the velocity fields, evaluated as Δu and Δv , as a function of radial position, for $\alpha = \pi/6, \pi/4$ and $\pi/3$. The slope markers show the predicted slopes of -2 (top) and $-8/3$ (bottom).

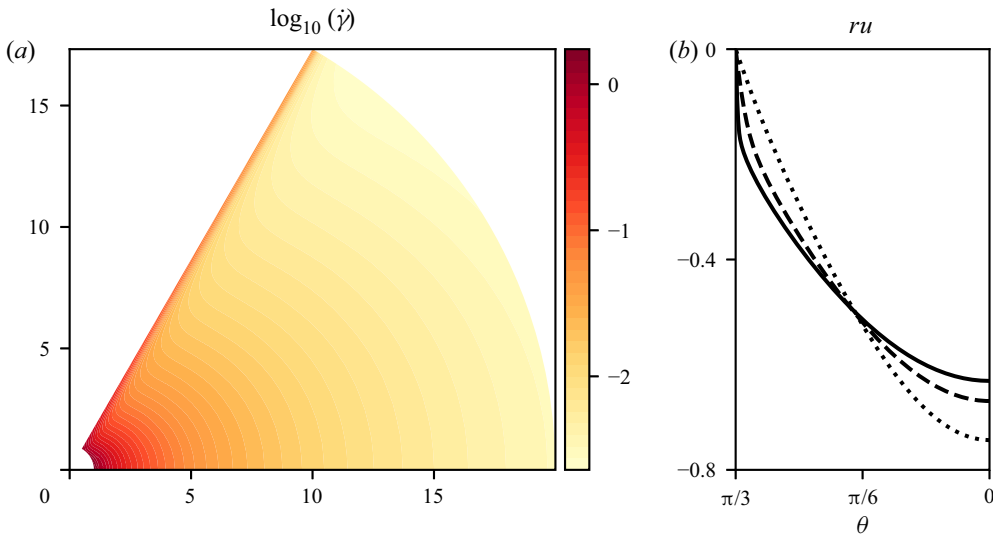


Figure 7. (a) A density plot of log strain rate from the $\alpha = \pi/3$ numerical simulation. (b) The scaled radial velocity, ru , as a function of angle, θ , for $\alpha = \pi/3$ and $r = 1$ (dotted), 4 (dashed) and 20 (solid). The θ axis is reversed so that the no-slip boundary is located at the left of the figure.

(with notation adjusted for consistency) before exploring it in greater detail by carrying out numerical integration not evaluated by Sandru & Camenshi (1979), and comparing to the results of direct numerical simulations in § 4.1.

In this regime the leading-order flow is given by the viscous solution (2.15a–c), which produces an $O(Bi)$ term in the stress. Hence the solution takes the form

$$u = u_0 + Bi u_1 + \dots, \quad v = Bi v_1 + \dots, \quad p = p_0 + Bi p_1 + \dots, \quad (4.1a-c)$$

with u_0 and p_0 given by (2.15a–c). By conservation of mass and for homogeneity in r at $O(Bi)$ in the expression of conservation of momentum, we define

$$u_1 = rf'(\theta) \quad \text{and} \quad v_1 = -2rf(\theta), \tag{4.2a,b}$$

where $f(\theta)$ is to be determined and $'$ denotes differentiation with respect to θ . Note that this r dependence of u_1 and v_1 was anticipated, due to the expansion parameter, in fact, being r^2Bi and the leading-order velocity depending upon r^{-1} . By eliminating pressure from the conservation of momentum equations, we find that $f(\theta)$ satisfies the differential equation

$$f'''(\theta) + 4f'(\theta) + H(\theta) = C, \tag{4.3}$$

where C is a constant of integration and

$$H(\theta) = \frac{d}{d\theta} \left(\frac{\sin 2\theta}{\sqrt{\sin^2 2\theta + (\cos 2\alpha - \cos 2\theta)^2}} \right) + \frac{2(\cos 2\theta - \cos 2\alpha)}{\sqrt{\sin^2 2\theta + (\cos 2\alpha - \cos 2\theta)^2}}. \tag{4.4}$$

The governing equation (4.3) is subject to four boundary conditions

$$f(0) = f''(0) = 0, \quad f(\alpha) = f'(\alpha) = 0, \tag{4.5a,b}$$

which represent symmetry at $\theta = 0$ and no slip at $\theta = \alpha$, which are sufficient to evaluate $f(\theta)$ and C . Having determined C , the pressure perturbation is given by

$$p_1 = C \ln(r) + \frac{1 + 2 \cos^2 2\alpha - 3 \cos 2\alpha \cos 2\theta}{\sqrt{\sin^2 2\theta + (\cos 2\theta - \cos 2\alpha)^2}} + \text{const.} \tag{4.6}$$

We integrate (4.3) numerically by first finding a particular solution from an initial value problem with initial conditions given at $\theta = 0$, then determining C and the coefficients of the complementary solution by the boundary conditions at α . Specifically, we find a solution of the form

$$f(\theta) = f_p(\theta) + \frac{C}{4}\theta + D \sin 2\theta, \tag{4.7}$$

where f_p is the unique solution to the initial value problem

$$f_p'''(\theta) + 4f_p'(\theta) + H(\theta) = 0, \tag{4.8}$$

subject to $f_p(0) = f_p'(0) = f_p''(0) = 0$. Then C and D are determined by the boundary conditions at $\theta = \alpha$

$$C = \frac{4(2f_p(\alpha) \cos 2\alpha - f_p'(\alpha) \sin 2\alpha)}{\sin 2\alpha - 2\alpha \cos 2\alpha} \quad \text{and} \quad D = \frac{\alpha f_p'(\alpha) - f_p(\alpha)}{\sin 2\alpha - 2\alpha \cos 2\alpha}. \tag{4.9a,b}$$

Velocity profiles for the first-order corrections to the leading-order viscous flow are given in figure 8. Note, again, the negative angular velocity, as anticipated. Also, the radial velocity is reduced at the centre of the wedge and enhanced towards the walls, as required to flatten the radial velocity profile as r increases. In this regime the magnitude of the corrections increases with increasing half-angle. This can be explained by considering the magnitude of the deviatoric stress in the leading-order solution,

$$\tau \equiv \sqrt{\tau_{rr}^2 + \tau_{r\theta}^2} = \frac{2\sqrt{1 + \cos^2 2\alpha - 2 \cos 2\theta \cos 2\alpha}}{r^2 (\sin 2\alpha - 2\alpha \cos 2\alpha)}, \tag{4.10}$$

which can be shown to decrease with increasing α . Thus, the fluid is less strongly stressed by the leading-order flow for larger wedge half-angles, and so the plasticity has a larger impact on the flow.

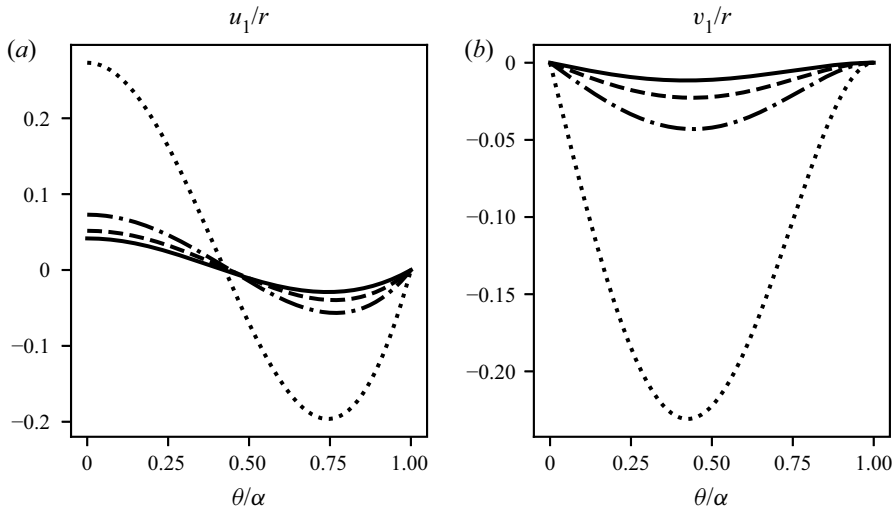


Figure 8. The first-order corrections to the velocities, u and v , in the viscous regime, as functions of the scaled angle, θ/α , for a wedge of half-angle $\alpha = \pi/6$ (solid), $\pi/4$ (dashed), $\pi/3$ (dash-dotted) and $\pi/2$ (dotted).

The additional shear stress at the wall due to the viscoplasticity in this regime is given by

$$Bi \tau_{r\theta}^{(1)} \Big|_{\theta=\alpha} = Bi + Bi \left(\frac{1}{r} \frac{\partial u_1}{\partial \theta} + \frac{\partial v_1}{\partial r} - \frac{v_1}{r} \right) \Big|_{\theta=\alpha} = Bi(f''(\alpha) + 1), \quad (4.11)$$

where $f''(\alpha)$ is determined numerically. This correction to the shear stress at the wall is plotted as a function of α in figure 9(a). An interesting feature of this profile is the minimum attained for an angle of $\alpha \approx 32^\circ$. The behaviour of the constant C is also of particular interest, as the first-order correction to the radial pressure gradient is given from (4.6) by $Bi C/r$. The behaviour of $C = r\partial p_1/\partial r$ as a function of α is given in figure 9(b), showing that C varies from 2.55 (approximately) at $\alpha = \pi/2$ and diverges as $\alpha \rightarrow 0$. In particular, we find that the perturbation to the shear stress at the wall, $\tau_{r\theta}^{(1)} \sim 3/2$, and $C \sim 3/(2\alpha)$ for $\alpha \ll 1$ as required for consistency with the plane Poiseuille solution in the limit $\alpha \rightarrow 0$ with $r\alpha = 1$ fixed (see Appendix D).

4.1. Numerical simulations

For numerical simulations in the viscous regime, a radial extent of $r \in [0.1, 10]$ and a range of small values for Bi were used. Again the simulations were run in FEniCS, on a mesh of 60 000 elements. Here, we imposed the purely viscous radial solution (2.15a–c) as Dirichlet boundary conditions at both inflow and outflow, and examined the flow profiles at $r = 1$, which was found to be sufficiently far from these boundaries not to be affected by the approximations made in the boundary conditions. Due to the low values of the Bingham number, all simulations were solved directly by Newton iteration from the purely radial Stokes solution (2.15a–c) converging to residuals of less than 10^{-8} .

Figure 10 shows example velocity profiles for $\alpha = \pi/4$, and with $Bi = 0.01$, demonstrating good agreement between asymptotic theory and numerical computation. As with the plastic regime, we measured the difference between the asymptotic profiles and the numerical solutions for $\alpha = \pi/6, \pi/4$ and $\pi/3$, this time at fixed $r = 1$ and variable Bi .

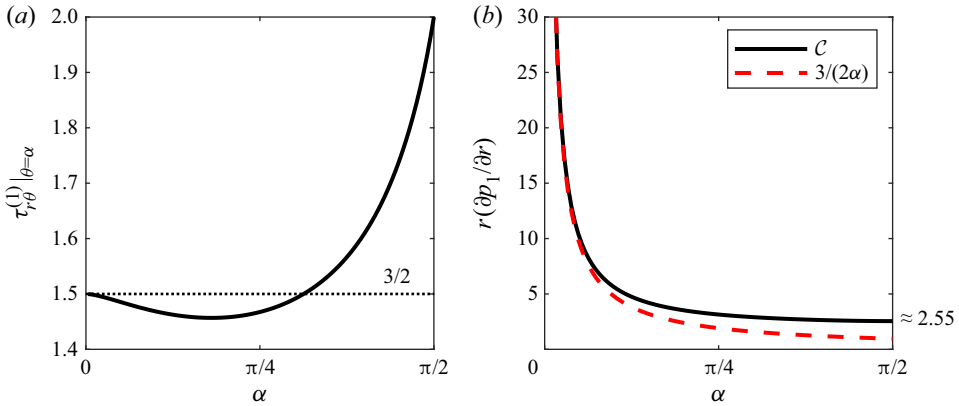


Figure 9. Features of the perturbation solution for the planar converging flow of a viscoplastic in the low Bingham number regime: (a) the additional wall shear stress, $\tau_{r\theta}^{(1)}|_{\theta=\alpha}$, and (b) the scaled additional radial pressure gradient, $r\partial p_1/\partial r = C$, as functions of wedge half-angle, α .

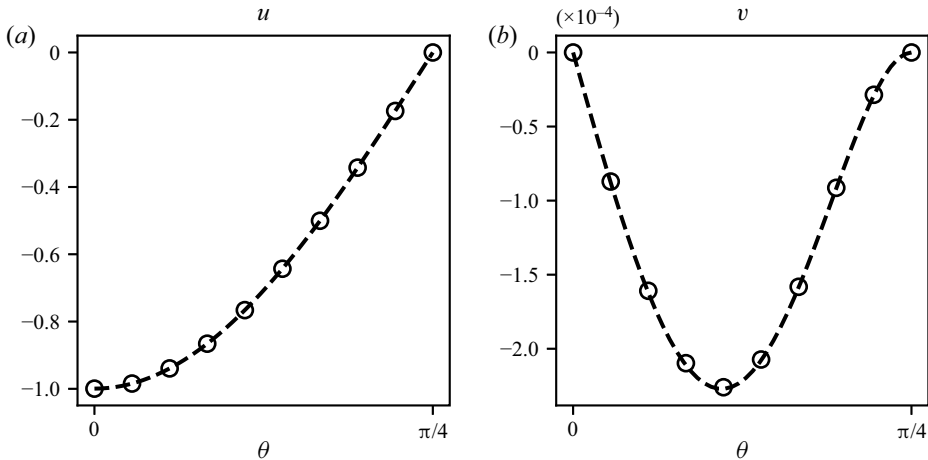


Figure 10. The asymptotic (dashed line) and numerical (circles) radial and angular velocities as functions of angle, θ , for $Bi = 0.01$ and $r = 1$. (a,b) Show the radial and angular profiles, respectively, for a wedge of half-angle $\alpha = \pi/4$.

With the absence of a boundary layer structure, there is no need for composite solutions, and so we measure the differences, Δu and Δv , between the first-order asymptotic expressions and the numerical solutions. Both differences were found to scale like Bi^2 , as expected having neglected second-order terms in the expansions.

5. Herschel–Bulkley flow

In this section we extend our examination of converging flows to Herschel–Bulkley fluids. Importantly, the key features of the boundary layer structure determined for Bingham fluids when $Bi \gg 1$ (§ 3) carry over to Herschel–Bulkley fluids and here we generalise our analysis to these materials. The Herschel–Bulkley viscoplastic model is defined by the

dimensional constitutive law

$$\boldsymbol{\tau} = \left(K\dot{\gamma}^{N-1} + \frac{\tau_c}{\dot{\gamma}} \right) \dot{\boldsymbol{\gamma}}, \quad (5.1)$$

where K is the consistency, N the flow index, and τ_c the yield stress. This model extends the Bingham model, which is reproduced for $N = 1$ and $K = \mu$, by allowing for shear thickening ($N > 1$) and shear thinning ($N < 1$). For this model we have the critical distance

$$r_c = \left(\frac{KQ^N}{\tau_c} \right)^{1/2N}, \quad (5.2)$$

above which the flow is dominated by plastic stresses. For a typical radial distance, R , we scale velocities by Q/R , strain rates by Q/R^2 and stresses and pressures by KQ^N/R^{2N} resulting in the non-dimensional constitutive equation

$$\begin{pmatrix} \tau_{rr} \\ \tau_{r\theta} \end{pmatrix} = \left(\dot{\gamma}^{N-1} + \frac{Bi}{\dot{\gamma}} \right) \begin{pmatrix} 2 \frac{\partial u}{\partial r} \\ \frac{1}{r} \frac{\partial u}{\partial \theta} + \frac{\partial v}{\partial r} - \frac{v}{r} \end{pmatrix}, \quad (5.3)$$

where the Bingham number is now given by

$$Bi = \frac{\tau_c R^{2N}}{KQ^N}. \quad (5.4)$$

The critical radial length scale is equivalent to asserting that the asymptotic analysis will break down for $r = O(Bi^{-1/2N})$ in non-dimensional variables.

In the $Bi \gg 1$ regime (or equivalently at large distances from the apex of the wedge), the bulk solution is unchanged at leading order since the viscous stresses are neglected here, and hence is given by (3.11)–(3.13). In the intermediate layer, using the same notation as for the Bingham case, albeit with a different small parameter, δ , the radial velocity takes the form

$$U = U_0(r) + \delta^{1/2} U_1(r, \zeta), \quad (5.5)$$

and the shear stress is given by

$$\tau_{r\theta} = -\frac{1}{r^N} \delta^{-N/2} |\partial_\zeta U_1|^{N-1} \partial_\zeta U_1 + Bi - 2r^2 \delta Bi \left(\frac{\partial_r U_0}{\partial_\zeta U_1} \right)^2 + \dots \quad (5.6)$$

Hence, a balance of viscous and plastic stresses is achieved in an intermediate layer of width δ , provided

$$\delta^{-N/2} = \delta Bi \implies \delta = Bi^{-2/(N+2)}, \quad (5.7)$$

and we find that U_1 satisfies the equation

$$|\partial_\zeta U_1|^{N+1} \partial_\zeta U_1 - 2cr^N \zeta |\partial_\zeta U_1|^2 + 2r^{N-2} \frac{A^2}{c^2} = 0, \quad (5.8)$$

where A and c are defined as previously for the bulk solution and given by (3.14) and (3.15). In the limit $\zeta \rightarrow -\infty$, $\partial_\zeta U_1 \rightarrow -\infty$ and leading-order terms of (5.8) then determine

$$\partial_\zeta U_1 = -r(-2c\zeta)^{1/N}, \quad (5.9)$$

which, integrated, reveals that the transition into the boundary layer occurs when

$$\delta^{1/2} \zeta^{(N+1)/N} = O(1), \tag{5.10}$$

or, equivalently, when

$$|\theta - \theta_Y| = O(\delta^{(N+2)/2(N+1)}) = O(Bi^{-1/(N+1)}). \tag{5.11}$$

Thus, the viscoplastic boundary layer is of thickness $\epsilon = Bi^{-1/(N+1)}$ (cf. Piau & Debiante 2004) and, after scaling, we have the boundary layer equation (using the same notation as in the Bingham problem)

$$\frac{\partial P}{\partial r} \equiv \frac{2c}{r} = \frac{1}{r^{N+1}} \frac{\partial}{\partial \tilde{\phi}} (|\partial_{\tilde{\phi}} \tilde{U}|^{N-1} \partial_{\tilde{\phi}} \tilde{U}), \tag{5.12}$$

which integrates to

$$\tilde{U} = \frac{N}{N+1} (2c)^{1/N} r [(\Phi - \tilde{\phi})^{(N+1)/N} - \Phi^{(N+1)/N}], \tag{5.13}$$

and matching to leading order at $\tilde{\phi} = \Phi$ implies that

$$\Phi(r) = \hat{\Phi} r^{-2N/(N+1)}, \tag{5.14}$$

where

$$\hat{\Phi} = \frac{1}{c} \left(\frac{(N+1)A}{N2^{1/N}} \right)^{N/(N+1)}. \tag{5.15}$$

The additional shear stress due to the viscoplastic boundary layer is given, to leading order, by

$$\begin{aligned} \left(\frac{1}{r^N} \left| \frac{\partial u}{\partial \theta} \right|^{N-1} \frac{\partial u}{\partial \theta} \right) \Big|_{\theta=\alpha} &= - \left(\frac{1}{\epsilon^N r^N} \left| \partial_{\tilde{\phi}} \tilde{U} \right|^{N-1} \partial_{\tilde{\phi}} \tilde{U} \right) \Big|_{\tilde{\phi}=0} \\ &= 2Bi^{N/(N+1)} c \Phi = Bi^{N/(N+1)} \left(\frac{2(N+1)A}{Nr^2} \right)^{N/(N+1)}. \end{aligned} \tag{5.16}$$

Using incompressibility, we find the polar velocity at the top of the boundary layer

$$v(r, \Theta = 1) = \epsilon \tilde{V}(r, \tilde{\phi} = \Phi) = -\epsilon r^{-(3N+1)/(N+1)} \frac{2N^3}{(2N+1)(N+1)^2} \hat{\Phi}^{(2N+1)/N} (2c)^{1/N}. \tag{5.17}$$

We note that the radial dependence of both the boundary layer width and the first-order corrections to the velocity field are consistent with expansions in $r^{2N}Bi$, as anticipated. Unlike for a Bingham fluid, the Cartesian thickness of the boundary layer, $r\epsilon\Phi(r) = \epsilon\hat{\Phi}r^{(1-N)/(1+N)}$, is dependent on r – growing with r for a shear-thinning fluid and decreasing for a shear-thickening fluid. This can be understood by considering the magnitude of the strain rate in the bulk, which decreases with r , resulting in a higher viscosity for a shear-thinning fluid, and effectively reducing the local Bingham number (the ratio of plastic and viscous stresses) relative to the global Bingham number, Bi . Since the boundary layer thickness increases with decreasing Bingham number, we find a larger

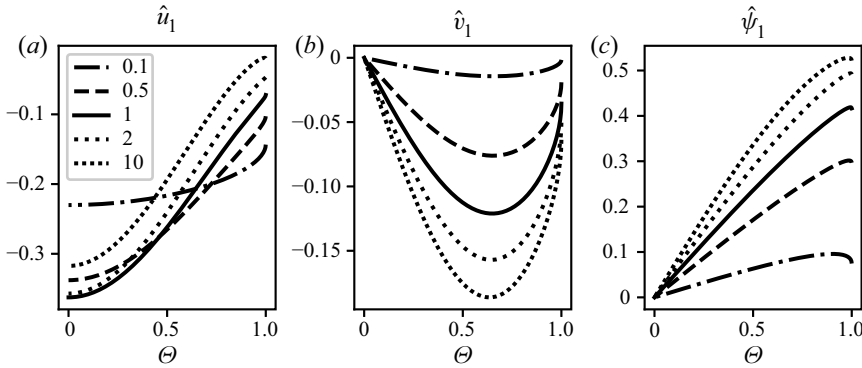


Figure 11. First-order corrections to the velocity and stress fields in the bulk as functions of the rescaled angle, Θ , for a Herschel–Bulkley fluid with flow index N (shown in legend). A solid line depicts the results for the Bingham model, $N = 1$. All solutions are for $\alpha = \pi/4$.

boundary layer thickness at larger distances from the apex for a shear-thinning fluid (and the reverse for a shear-thickening fluid).

Provided $\epsilon \gg Bi^{-1}$, as is the case for $N > 0$, the first-order correction to the bulk solution is found at an order before viscous stresses need to be considered. Hence, we can proceed to solve for these corrections as in § 3.5. The dependent variables in the bulk are given by the following series expansions:

$$\psi = \psi_0(\Theta) + \epsilon r^{-2N/(N+1)} \hat{\psi}_1(\Theta) + \dots, \tag{5.18}$$

$$u = \frac{\hat{u}_0(\Theta)}{r} + \epsilon r^{-(3N+1)/(N+1)} \hat{u}_1(\Theta) + \dots, \tag{5.19}$$

$$v = \epsilon r^{-(3N+1)/(N+1)} \hat{v}_1(\Theta) + \dots, \tag{5.20}$$

and following through the analysis with the new expression for Φ gives a similar set of ODEs to those for the Bingham case, (3.46)–(3.48). These equations, along with the asymptotic behaviour at $\Theta = 1$, are detailed in Appendix B. They are numerically integrated using a shooting technique as in § 3.5.

Example profiles of the first-order corrections, for $\alpha = \pi/4$ and different values of N , are given in figure 11. The general dependence of these profiles on N can be explained as follows. For a shear-thinning (thickening) fluid, the high shear at the walls results in a lower (higher) effective viscosity, allowing the pressure gradient to support higher (lower) shear rates and a thinner (thicker) boundary layer, resulting in a smaller (larger) adjustment to the leading-order plastic velocities and stresses in the bulk of the wedge. The velocity in the radial direction depends on N in a non-trivial way. For a small flow index, for which the constitutive law is almost plastic, the profile is largely independent of Θ , corresponding to a reasonably plastic-like velocity profile. As the index increases the profile becomes more strongly sheared and, above some value of the flow index, the magnitude of the radial flow enhancement also reduces.

6. Bingham fluid in a cone

In this section we examine converging flow of a Bingham fluid through an axisymmetric cone. The results obtained for the two-dimensional flow through a wedge are generalised to this three-dimensional setting. Importantly, we find that viscoplasticity induces angular

velocity away from the boundaries towards the axis of the cone and enhances boundary shear stress, and, when the material is only weakly yielded in the bulk, viscoplastic boundary layers develop. The conical geometry, however, introduces some algebraic complexity to the governing equations and asymptotic solution.

In the axisymmetric conical geometry we employ spherical coordinates, (r, θ, ϕ) , where r is the distance from the apparent vertex of the cone, $\theta \in [0, \pi]$ is now the polar angle measured from the axis of symmetry of the cone, and $\phi \in [0, 2\pi]$ is the azimuthal angle measured from an arbitrary choice of axis perpendicular to the axis of symmetry. The rigid walls are located at $\theta = \alpha$, the half-angle of the cone, and we assume independence of ϕ and no flow in the ϕ direction. Thus, we define the velocity components as $\mathbf{u} = (u, v, 0)$.

This problem is characterised by the following dimensional parameters (and for clarity of exposition we focus only on the Bingham rheology): density, ρ , viscosity, μ , yield stress, τ_c , typical radial distance from the apex, R , and the volume flux, \mathcal{Q} . (We note that, for flow in a cone, the volume flux, \mathcal{Q} , is dimensionally distinct from the volume flux per unit width in a wedge, \mathcal{Q}). The flow variables are rendered dimensionless as follows: velocities are scaled by \mathcal{Q}/R^2 , strain rates by \mathcal{Q}/R^3 and stresses and pressures by $\mu \mathcal{Q}/R^3$. The resulting non-dimensional equations are

$$\frac{1}{r^2} \frac{\partial}{\partial r}(r^2 u) + \frac{1}{r \sin \theta} \frac{\partial}{\partial \theta}(v \sin \theta) = 0, \tag{6.1}$$

$$\frac{\partial p}{\partial r} = \frac{\partial \tau_{rr}}{\partial r} + \frac{1}{r} \frac{\partial \tau_{r\theta}}{\partial \theta} + \frac{3}{r} \tau_{rr} + \frac{\cot \theta}{r} \tau_{r\theta}, \tag{6.2}$$

$$\frac{1}{r} \frac{\partial p}{\partial \theta} = \frac{\partial \tau_{r\theta}}{\partial r} + \frac{1}{r} \frac{\partial \tau_{\theta\theta}}{\partial \theta} + \frac{3}{r} \tau_{r\theta} + \frac{\cot \theta}{r} (\tau_{\theta\theta} - \tau_{\phi\phi}), \tag{6.3}$$

$$\boldsymbol{\tau} = \left(1 + \frac{Bi}{\dot{\gamma}}\right) \dot{\boldsymbol{\gamma}}, \tag{6.4}$$

$$\dot{\gamma}_{rr} = 2 \frac{\partial u}{\partial r}, \quad \dot{\gamma}_{r\theta} = \frac{1}{r} \frac{\partial u}{\partial \theta} + \frac{\partial v}{\partial r} - \frac{v}{r}, \quad \dot{\gamma}_{\theta\theta} = \frac{2}{r} \frac{\partial v}{\partial \theta} + \frac{2u}{r}, \quad \dot{\gamma}_{\phi\phi} = \frac{2v \cot \theta}{r} + \frac{2u}{r}, \tag{6.5a-d}$$

$$\dot{\gamma} = \sqrt{\frac{1}{2}(\dot{\gamma}_{rr}^2 + \dot{\gamma}_{\theta\theta}^2 + \dot{\gamma}_{\phi\phi}^2 + 2\dot{\gamma}_{r\theta}^2)}, \tag{6.6}$$

representing incompressibility (6.1), conservation of momentum in the radial and polar directions (6.2) and (6.3), the Bingham constitutive law (6.4) and the definition of the non-zero components and second invariant of the strain-rate tensor (6.5a-d) and (6.6). The Bingham number for this problem is given by

$$Bi = \frac{R^3 \tau_c}{\mu \mathcal{Q}}. \tag{6.7}$$

Again, due to this dependence of the Bingham number on R , we anticipate the expansions to proceed as functions of $r^3 Bi$. Now we have the critical length scale, $r_c = (\mu \mathcal{Q}/\tau_c)^{1/3}$. The plastically dominated regime, $Bi \gg 1$, corresponds to the dimensional distance from the apex of the cone being significantly larger than r_c , and the viscously dominated regime, $Bi \ll 1$, occurs for radial distances much smaller than r_c . The Reynolds number is given by $Re = \rho \mathcal{Q}/(\mu R)$, and again for the following it will be sufficient that $Re = O(1)$ and $Re \ll Bi$, to neglect inertial terms in the $Bi \gg 1$ and $Bi \ll 1$ regimes, respectively. We note that, unlike the planar problem, the Reynolds number also has radial dependence and

The converging flow of viscoplastic fluid

so, for given material parameters and volume flux, it will not be possible to neglect inertial terms for arbitrarily small distances from the apex of the cone.

The equations (6.1)–(6.3) are to be solved subject to boundary conditions

$$u = v = 0 \text{ at } \theta = \alpha, \quad v = \frac{\partial u}{\partial \theta} = 0 \text{ at } \theta = 0, \quad (6.8a,b)$$

corresponding to no slip and axisymmetry, respectively. We additionally have the integral expression for the volume flux,

$$2\pi \int_0^\alpha r^2 u \sin \theta \, d\theta = -1. \quad (6.9)$$

The corresponding problem for a rigid plastic was solved by Shield (1955), assuming purely radial flow and a radially independent deviatoric stress state. The solution corresponds closely to Nadai's solution for a planar wedge, and to make the correspondence clearer we adjust Shield's notation slightly by parameterising the non-zero components of the deviatoric stress via

$$\tau_{rr} = \frac{2}{\sqrt{3}} Bi \cos 2\psi, \quad \tau_{\theta\theta} = \tau_{\phi\phi} = -\frac{1}{\sqrt{3}} Bi \cos 2\psi, \quad \tau_{r\theta} = Bi \sin 2\psi, \quad \psi = \psi(\theta), \quad (6.10a-d)$$

which ensures that the deviatoric stress tensor is trace free and everywhere has constant second invariant, Bi . The equality of $\tau_{\theta\theta}$ and $\tau_{\phi\phi}$ is a consequence of the purely radial flow.

The solution is then given by

$$u = -\frac{\mathcal{A}}{r^2} \exp\left(-2\sqrt{3} \int_0^\theta \tan 2\psi \, d\theta\right), \quad \frac{\partial p}{\partial r} = \frac{2cBi}{r}, \quad (6.11a,b)$$

$$\psi'(\theta) = c \sec 2\psi - \sqrt{3} - \frac{1}{2} \cot \theta \tan 2\psi, \quad (6.12)$$

where c is determined by the boundary conditions

$$\psi(0) = 0, \quad \psi(\alpha) = \frac{\pi}{4}, \quad (6.13a,b)$$

and \mathcal{A} is determined by the flux condition (6.9).

The viscous problem of purely radial converging flow in a cone was first solved by Harrison (1919), and later explored in great detail by Ackerberg (1965), who found that the inclusion of inertial terms resulted in non-radial solutions occurring at the outflow of the cone. For vanishing Reynolds number, as considered by Harrison (1919), the problem is more straightforward, with a purely radial solution given by

$$u = \frac{3}{2\pi r^2} \frac{\cos^2 \alpha - \cos^2 \theta}{(1 - \cos \alpha)^2 (1 + 2 \cos \alpha)}, \quad p = \frac{1}{\pi r^3} \frac{1 - 3 \cos^2 \theta}{(1 - \cos \alpha)^2 (1 + 2 \cos \alpha)} + \text{const.} \quad (6.14a,b)$$

As with the planar wedge, the viscous velocity profile (6.14a,b) exhibits enhanced velocity in the centre of the wedge, compared to the perfectly plastic velocity profile (6.11a,b). As the fluid flows from large to small distances from the apex, the strain rate increases due to the converging nature of the flow, and the material evolves from plastically dominated to viscously dominated behaviour. Thus, superimposed upon the radial dependence of the

flow due to the converging geometry, we expect an additional acceleration at the centre of the cone, and velocity reduction at the outer surface of the cone. Conservation of mass then requires a flow of the fluid in the negative polar direction, towards the centre of the cone and away from the walls, and the quantification of this velocity field is a significant outcome of this analysis.

6.1. The plastic regime

The plastic solution (6.11a,b) and (6.12) does not satisfy no slip on the boundary of the cone, and the strain rate becomes unbounded here. So, for a viscoplastic fluid in the plastic regime, $Bi \gg 1$ (or equivalently, sufficiently far from the apex), we construct a viscoplastic boundary layer and intermediate layer, as for the wedge solution. Since the boundary layer and intermediate region are relatively thin, the curvature in the ϕ direction is negligible and the equations and solutions are identical to the planar geometry in these regions. In particular, we have the same boundary layer thickness, $\epsilon = Bi^{-1/2}$, and intermediate region thickness, $\delta = Bi^{-2/3}$. On the other hand, the r dependent terms, Φ , U_0 and V_0 , which are determined from matching with the bulk solution, differ.

In the bulk, we use the same strained coordinate approach, defining

$$\theta = (\alpha - \epsilon\Phi)\Theta, \tag{6.15}$$

and velocity expansions

$$u = u_0 + \epsilon u_1 + \dots, \quad v = \epsilon v_1 + \dots \tag{6.16a,b}$$

However, we need to introduce a different parameterisation of the deviatoric stress, which allows for a weak flow in the polar direction, and hence a non-zero normal stress difference, $\tau_{\theta\theta} - \tau_{\phi\phi}$. One such parameterisation is

$$\frac{\tau_{rr}}{Bi} = \frac{2}{\sqrt{3}} \cos 2\psi \cos 2\chi, \quad \frac{\tau_{\theta\theta}}{Bi} = -\frac{1}{\sqrt{3}} \cos 2\psi \cos 2\chi + \cos 2\psi \sin 2\chi, \tag{6.17a,b}$$

$$\frac{\tau_{\phi\phi}}{Bi} = -\frac{1}{\sqrt{3}} \cos 2\psi \cos 2\chi - \cos 2\psi \sin 2\chi, \quad \frac{\tau_{r\theta}}{Bi} = \sin 2\psi, \tag{6.18a,b}$$

which reduces to the previous parameterisation (6.10a-d) for $\chi = 0$ and gives all possible symmetric, trace-free stress states satisfying $\tau \equiv \sqrt{\tau_{ij}\tau_{ij}}/2 = Bi$, and $\tau_{r\phi} = \tau_{\theta\phi} = 0$. We define asymptotic series for ψ and χ by

$$\psi = \psi_0(r) + \epsilon\psi_1(r, \theta) + \dots, \quad \chi = \epsilon\chi_1(r, \theta) + \dots, \tag{6.19a,b}$$

so that, at $O(1)$, $\chi = 0$ and the stress decomposition is precisely that given in (6.10a-d), for the purely radial solution.

With the coordinate transform (6.15), the full governing equations (6.1)–(6.6) can be reduced to

$$\frac{1}{r}L_r(r^2u) + L_\Theta v + v \cot(\alpha\Theta - \epsilon\Phi\Theta) = 0, \tag{6.20}$$

$$(L_\Theta L_r + 3L_\Theta)\tau_{rr} + (L_\Theta^2 - L_r^2 - 3L_r)\tau_{r\theta} - L_r L_\Theta \tau_{\theta\theta} + L_\Theta (\cot(\alpha\Theta - \epsilon\Phi\Theta)\tau_{r\theta}) - L_r (\cot(\alpha\Theta - \epsilon\Phi\Theta)(\tau_{\theta\theta} - \tau_{\phi\phi})) = 0, \tag{6.21}$$

$$2\tau_{r\theta}L_r u = \tau_{rr}(L_\Theta u + L_r v - v), \tag{6.22}$$

$$2\tau_{\theta\theta}L_r u = \tau_{rr}(2L_\Theta v + 2u). \tag{6.23}$$

The converging flow of viscoplastic fluid

Here, (6.20) is conservation of mass, (6.21) is the curl of the momentum balances and (6.22) and (6.23) are a statement of the proportionality between corresponding components of the deviatoric stress and strain-rate tensors. The linear operators, L_r and L_Θ , are given by

$$L_r = r \frac{\partial}{\partial r} + \frac{\epsilon r \Phi' \Theta}{\alpha} \frac{\partial}{\partial \Theta}, \quad L_\Theta = \frac{1}{\alpha - \epsilon \Phi} \frac{\partial}{\partial \Theta} = \left(\frac{1}{\alpha} + \frac{\epsilon \Phi}{\alpha^2} + \dots \right) \frac{\partial}{\partial \Theta}. \quad (6.24a,b)$$

Expansion of the governing equations at $O(1)$ gives the equivalent of Shield's solution

$$u_0 := \frac{\hat{u}_0}{r^2} = -\frac{\mathcal{A}}{r^2} \exp\left(-2\sqrt{3} \int_0^\Theta \alpha \tan 2\psi_0 \, d\Theta\right), \quad \frac{\partial p_0}{\partial r} = \frac{2cBi}{r}, \quad (6.25a,b)$$

$$\psi_0'(\Theta) = \alpha(c \sec 2\psi_0 - \sqrt{3} - \frac{1}{2} \cot \alpha \Theta \tan 2\psi_0), \quad (6.26)$$

where c is determined by the boundary conditions

$$\psi_0(0) = 0, \quad \psi_0(1) = \frac{\pi}{4}, \quad (6.27a,b)$$

and \mathcal{A} is determined by the flux condition

$$2\pi\alpha \int_0^1 \hat{u}_0(\Theta) \sin \alpha \Theta \, d\Theta = 1. \quad (6.28)$$

We define $\hat{U}_0 = \hat{u}_0(\Theta = 1)$ since, unlike for the planar solution, this does not have a closed-form expression in terms of \mathcal{A} and c . We note that this solution (6.25a,b)–(6.28) exhibits a non-vanishing radial velocity and a divergent shear rate as $\Theta \rightarrow 1$, just as for the flow through a planar wedge. We therefore must introduce both the intermediate and boundary layers in order to enforce the boundary conditions. However, this matching is identical to §§ 3.3 and 3.4 and we deduce that

$$\Phi(r) \equiv \frac{\hat{\Phi}}{r^{3/2}} = \sqrt{-\frac{\hat{U}_0}{cr^3}}, \quad V_0(r) = -\frac{cr\Phi^3}{3} = -\frac{c\hat{\Phi}^3}{3} r^{-7/2}. \quad (6.29a,b)$$

Thus, the boundary layer width scales like $(r^3 Bi)^{-1/2}$ and the first-order corrections to the velocities scale like $r^{-2}(r^3 Bi)^{-1/2}$, as expected given the true expansion parameter $r^3 Bi$. We may now use these expressions to calculate the effect of the boundary layer in the bulk, and, in particular, the induced angular velocity. To do so we define

$$u_1 = r^{-7/2} \hat{u}_1(\Theta), \quad v_1 = r^{-7/2} \hat{v}_1(\Theta), \quad \psi_1 = r^{-3/2} \hat{\psi}_1(\Theta), \quad \chi_1 = r^{-3/2} \hat{\chi}_1(\Theta), \quad (6.30a-d)$$

and expand the governing equations (6.20)–(6.23) at order ϵ to obtain four ODEs for \hat{u}_1 , \hat{v}_1 , $\hat{\psi}_1$ and $\hat{\chi}_1$:

$$-\frac{3}{2}\hat{u}_1 + \frac{1}{\alpha}\hat{v}'_1 + \hat{v}_1 \cot \alpha\Theta = \frac{3\hat{\Phi}\Theta}{2\alpha}\hat{u}'_0, \tag{6.31}$$

$$\begin{aligned} &\frac{2}{\alpha^2}(\hat{\psi}_1 \cos 2\psi_0)'' + \frac{3}{\alpha}(\hat{\chi}_1 \cos 2\psi_0)' - \frac{\sqrt{3}}{\alpha}(\hat{\psi}_1 \sin 2\psi_0)' + \frac{2}{\alpha}(\hat{\psi}_1 \cot \alpha\Theta \cos 2\psi_0)' \\ &+ \left(\frac{9}{2}\hat{\psi}_1 + 6\hat{\chi}_1 \cot \alpha\Theta\right) \cos 2\psi_0 = \frac{\hat{\Phi}}{\alpha^2} \left(\frac{3\sqrt{3}\Theta}{2}(\cos 2\psi_0)'' - \sqrt{3}(\cos 2\psi_0)'\right. \\ &\left. - \frac{2}{\alpha}(\sin 2\psi_0)'' - \frac{9\alpha\Theta}{4}(\sin 2\psi_0)' - ((\cot \alpha\Theta + \alpha\Theta \operatorname{cosec}^2 \alpha\Theta) \sin 2\psi_0)'\right), \end{aligned} \tag{6.32}$$

$$\begin{aligned} &-7\sqrt{3}\hat{u}_1 \tan 2\psi_0 - \frac{2}{\alpha}\hat{u}'_1 + 9\hat{v}_1 - 8\sqrt{3}\hat{\psi}_1\hat{u}_0 + \frac{4}{\alpha}\hat{\psi}_1\hat{u}'_0 \tan 2\psi_0 \\ &= \frac{\hat{\Phi}}{\alpha^2}(3\sqrt{3}\alpha\Theta \tan 2\psi_0 + 2)\hat{u}'_0, \end{aligned} \tag{6.33}$$

$$3\hat{u}_1 - \frac{4}{\alpha}\hat{v}'_1 - 8\sqrt{3}\hat{\chi}_1\hat{u}_0 = -\frac{3\hat{\Phi}\Theta}{\alpha}\hat{u}'_0, \tag{6.34}$$

with boundary conditions

$$\hat{\psi}_1 = \hat{v}_1 = 0 \text{ at } \Theta = 0, \quad \hat{v}_1 = -\frac{c\hat{\Phi}^3}{3} \text{ at } \Theta = 1, \tag{6.35a,b}$$

from symmetry at $\Theta = 0$ and matching to the boundary layer solution at $\Theta = 1$. As in the planar case, matching of τ_{rr} to the intermediate layer requires

$$\hat{\psi}_1 = \frac{3\sqrt{3}\hat{\Phi}}{4} \text{ at } \Theta = 1. \tag{6.36}$$

Similarly, analysis of the normal stress difference, $\tau_{\theta\theta} - \tau_{\phi\phi}$, in the intermediate layer gives

$$\begin{aligned} \tau_{\theta\theta} - \tau_{\phi\phi} &\equiv \left(1 + \frac{Bi}{\dot{\gamma}}\right) \left(\frac{2}{r} \frac{\partial v}{\partial \theta} - \frac{2v}{r} \cot \theta\right) \\ &= \left(-\frac{Bi}{\frac{1}{r\sqrt{\delta}} \frac{\partial U_1}{\partial \zeta}} + \dots\right) \left(\frac{2\epsilon r \Phi'}{r\sqrt{\delta}} \frac{\partial U_1}{\partial \zeta} + \dots\right) = 3Bi^{1/2}\Phi + \dots, \end{aligned} \tag{6.37}$$

using (3.20), (3.28) and the identity $r\Phi' = -3\Phi/2$. While in the bulk solution

$$\tau_{\theta\theta} - \tau_{\phi\phi} \equiv 2Bi \cos 2\psi \sin 2\chi = 4Bi^{1/2}\chi_1 \sqrt{2\alpha(2c - \cot \alpha)(1 - \Theta)} + \dots, \tag{6.38}$$

as $\Theta \rightarrow 1$, using the behaviour of ψ_0 in the neighbourhood of $\Theta = 1$ (see Appendix C). Thus, $\hat{\chi}_1$ diverges like $(1 - \Theta)^{-1/2}$ as $\Theta \rightarrow 1$, which is consistent with the leading-order behaviour of $\hat{\chi}_1$ from the differential equations (6.31)–(6.34) close to $\Theta = 1$.

The converging flow of viscoplastic fluid

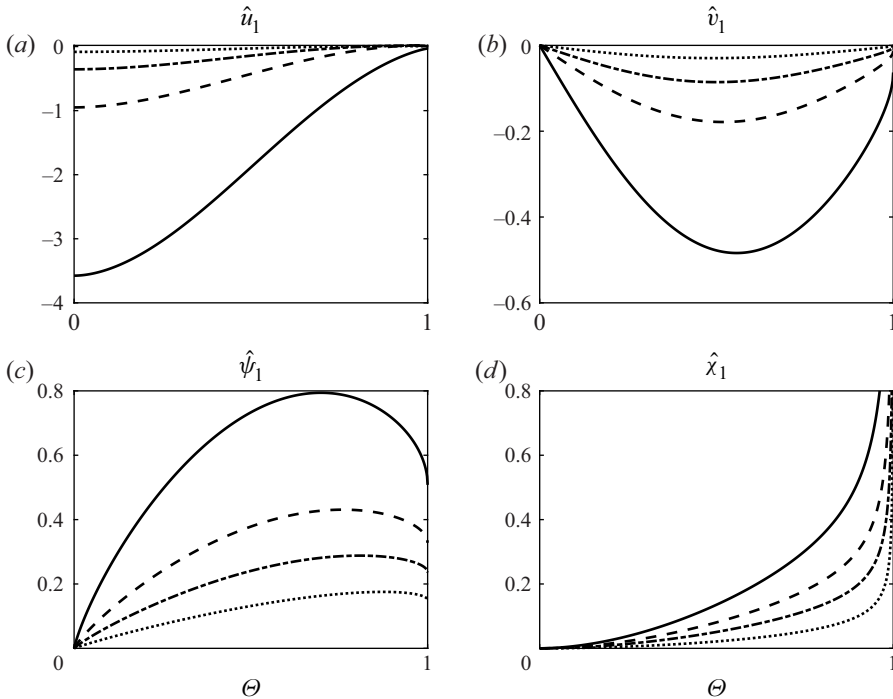


Figure 12. The first-order corrections to the velocities, u and v , and the stress orientation functions, ψ and χ , for viscoplastic flow in a cone in the plastic regime, as functions of the scaled polar coordinate Θ , for $\alpha = \pi/6$ (solid), $\pi/4$ (dashed), $\pi/3$ (dash-dotted) and $\pi/2$ (dotted).

Although the divergence of $\hat{\chi}_1$ may seem problematic for the asymptotic order of our expansions, we expect the plastic regime to break down within the intermediate layer, for which $1 - \Theta = O(\delta)$. Here, we have $\chi = O(\epsilon\delta^{-1/2}) \ll 1$, since $\delta \gg \epsilon^2$, and so χ remains small throughout the region of validity of the plastic equations. The reason for this divergence of the normal stress difference is that the gradient of the polar velocity, $\partial v/\partial\theta$, becomes large in the boundary layer, while the polar velocity itself remains small, thus $\tau_{\theta\theta}$ becomes significantly larger than $\tau_{\phi\phi}$.

The boundary-value problem given by (6.31)–(6.36) was again solved by a shooting method. In this situation we have potential singularities at both ends of the domain, due to the $\cot\alpha\Theta$ terms, so asymptotic analysis was required to step a small distance away from $\Theta = 0$ and $\Theta = 1$ (see (C4)–(C8) in Appendix C) before numerically shooting towards the centre of the domain, and fixing unknown coefficients by enforcing continuity at some central point. Again, the solutions were found to be essentially identical for sufficiently small choices of the step sizes, and the method converges effectively for any sufficiently central choice of matching point. The profiles given in figure 12 were produced with a step size of $d = 10^{-8}$ away from the singularities at both ends of the domain, and with matching point at $\Theta = 0.5$.

From the solutions to the boundary-value problem, we find that the velocity profiles are qualitatively similar to those for the planar wedge (figure 3), with a negative polar velocity out from the boundary layer towards the centre of the cone and an enhancement of the velocity in the radial direction, both of which are increased for decreasing half-angle, due to the boundary layer thickness, $\hat{\phi}$, increasing for decreasing α . The shear stress is again enhanced throughout the domain, due to the greater shear stress at the wall, and we find

that the normal stress difference becomes significant at the edge of the boundary layer, $\Theta = 1$, via the divergence of $\hat{\chi}_1$, as discussed above.

6.2. The viscous regime

The viscous regime, $Bi \ll 1$, can be tackled by expanding the governing equations around the leading-order Stokes solution. We define the asymptotic series

$$u = u_0 + Bi u_1 + \dots, \quad v = Bi v_1 + \dots, \quad p = p_0 + Bip_1 + \dots, \quad (6.39a-c)$$

where u_0 and p_0 are given by (6.14a,b). For homogeneity in r in the perturbation to the stress tensor, and using conservation of mass, we can write

$$u_1 \equiv r\hat{u}_1(\theta) = \frac{r}{\sin\theta} g'(\theta), \quad v_1 \equiv r\hat{v}_1(\theta) = -\frac{3}{\sin\theta} g(\theta), \quad (6.40a,b)$$

where g is a function to be determined, and $'$ represents differentiation with respect to θ . From the expression of conservation of momentum in the angular direction at $O(Bi)$, we find that the angular pressure gradient is independent of r , and so the radial pressure gradient is independent of θ , giving

$$r \frac{\partial p_1}{\partial r} = \mathcal{H}(\theta) + \frac{1}{\sin\theta} g''' - \frac{\cos\theta}{\sin^2\theta} g'' + \frac{1 + 6 \sin^2\theta}{\sin^3\theta} g' = \mathcal{C}, \quad (6.41)$$

where \mathcal{C} is an arbitrary constant, to be determined, and $\mathcal{H}(\theta)$ is given by

$$\mathcal{H}(\theta) = \frac{d}{d\theta} \left(\frac{\sin 2\theta}{\sqrt{\sin^2 2\theta + 3(\cos 2\theta - \cos 2\alpha)^2}} \right) + \frac{2 \cos^2 \theta + 6 \cos 2\theta - 6 \cos 2\alpha}{\sqrt{\sin^2 2\theta + 3(\cos 2\theta - \cos 2\alpha)^2}}. \quad (6.42)$$

Thus we have the third-order ODE,

$$g''' - \cot\theta g'' + (6 + \operatorname{cosec}^2\theta)g' = (\mathcal{C} - \mathcal{H}(\theta)) \sin\theta. \quad (6.43)$$

For $\hat{u}_1(0)$ to remain finite, we need $g(0) = 0$. For symmetry we require g to be an even function of θ , which ensures u_1 is even and v_1 is odd. Finally, we have the no-slip boundary condition at the wall, which gives

$$g(\alpha) = g'(\alpha) = 0. \quad (6.44)$$

To solve the ODE numerically we shoot from $\theta = d \ll 1$, to avoid the potential singularity at $\theta = 0$, with initial conditions

$$g(d) = \lambda d^2, \quad g'(d) = 2\lambda d, \quad g''(d) = 2\lambda, \quad (6.45a-c)$$

and determine λ and \mathcal{C} by enforcing the two boundary conditions at $\theta = \alpha$, (6.44). The solutions are found to be essentially independent of d for $d < 10^{-5}$. Profiles of \hat{u}_1 and \hat{v}_1 are given in figure 13, demonstrating the anticipated negative polar velocity away from the boundary and towards the centre of the cone. As in the planar case, the first-order corrections are larger for larger α , due to the magnitude of the deviatoric stress in the leading-order viscous solution being smaller at larger half-angles, resulting in a less yielded fluid and more significant plasticity effects.

The converging flow of viscoplastic fluid

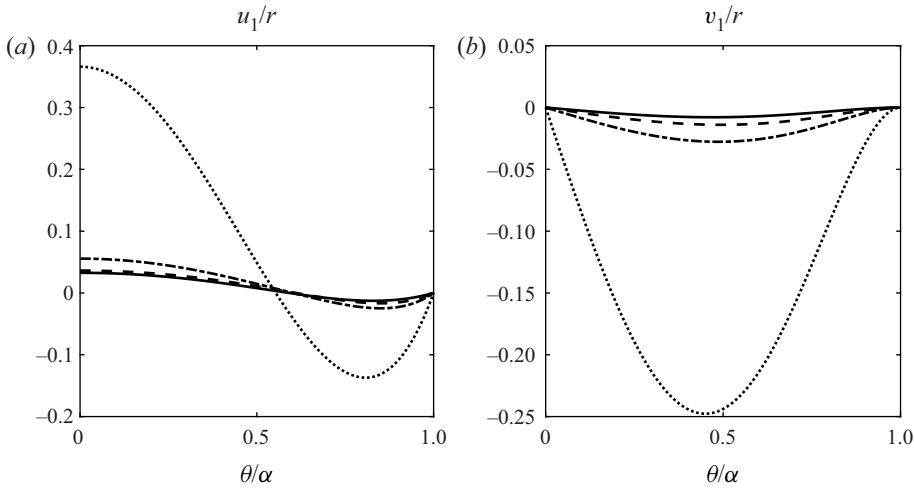


Figure 13. The first-order corrections to the velocities, u and v , for viscoplastic flow in a cone in the viscous regime, as functions of the scaled polar coordinate θ/α , for $\alpha = \pi/6$ (solid), $\pi/4$ (dashed), $\pi/3$ (dash-dotted) and $\pi/2$ (dotted).

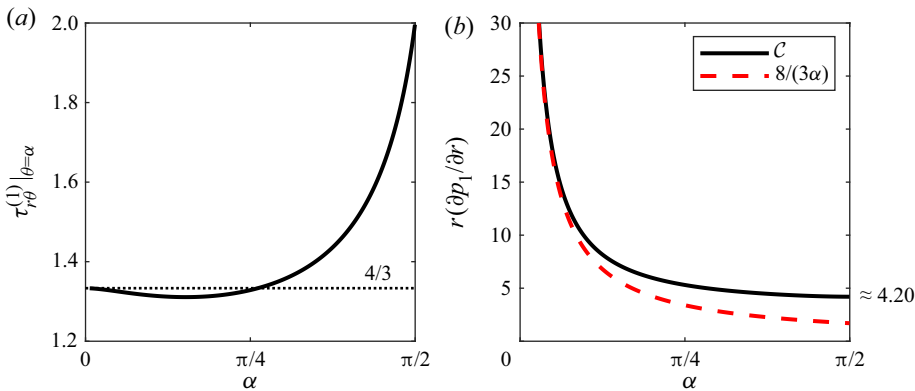


Figure 14. Features of the perturbation solution for the conical converging flow of a viscoplastic in the low Bingham number regime: (a) the additional wall shear stress, $\tau_{r\theta}^{(1)}|_{\theta=\alpha}$, and (b) the scaled additional radial pressure gradient, $r\partial p_1/\partial r = \mathcal{C}$, as functions of cone half-angle, α .

The additional shear stress at the wall is given by

$$Bi \tau_{r\theta}^{(1)}|_{\theta=\alpha} = Bi + Bi \left(\frac{1}{r} \frac{\partial u_1}{\partial \theta} + \frac{\partial v_1}{\partial r} - \frac{v_1}{r} + 1 \right) \Big|_{\theta=\alpha} = Bi \left(\frac{g''(\alpha)}{\sin \alpha} + 1 \right), \quad (6.46)$$

which is plotted as a function of α in figure 14a), demonstrating a similar behaviour to that for the planar wedge, with a minimum attained for a slightly smaller half-angle of $\alpha \approx 27^\circ$. The constant \mathcal{C} is also of interest since the first-order correction to the radial pressure gradient is given by $Bi\mathcal{C}/r$, thus the behaviour of $\mathcal{C} = r\partial p_1/\partial r$ with α is given in figure 14b), showing that \mathcal{C} varies from 4.20 (approximately) at $\alpha = \pi/2$ and diverges as $\alpha \rightarrow 0$. In particular, we find that the perturbation to the shear stress at the wall, $\tau_{r\theta}^{(1)} \sim 4/3$, and $\mathcal{C} \sim 8/(3\alpha)$ for $\alpha \ll 1$ as required for consistency with the pipe Poiseuille solution in the limit $\alpha \rightarrow 0$ with $r\alpha = 1$ fixed (see Appendix D).

7. Discussion and conclusions

Asymptotic solutions have been found for the converging flow of a viscoplastic fluid through a planar wedge and conical geometry, in the plastically and viscously dominated regimes, and verified for the case of a Bingham fluid in a wedge using direct finite element simulations. A key feature in both regimes is that no purely radial solution is possible. Instead, a weak angular flow is induced away from the boundaries and towards the centre of the domains. This result can be explained as a consequence of mass conservation as the fluid flows from a plastically dominated to viscously dominated velocity profile, experiencing enhanced flow velocity at the centre of the domain and reduced velocity near the walls as a consequence of no-slip conditions.

In the plastically dominated regime ($Bi \gg 1$) for a Bingham fluid, thin viscoplastic boundary layers of width $\epsilon = Bi^{-1/2}$ are required at the walls, allowing the flow to satisfy no slip. The angular extent of these boundary layers also depends on the radial distance from the apparent apex, r , scaling as ϵr^{-1} in a wedge and $\epsilon r^{-3/2}$ in a cone. Additionally, an intermediate asymptotic layer is required to regularise divergent strain rates close to the wall. The weak angular flow, induced by the boundary layer, is also $O(\epsilon)$ and both the boundary layer and angular flow are weaker for larger half-angles. The shear stress is enhanced compared to the rigid plastic solution, exceeding the yield stress by $O(\epsilon Bi)$ at the walls.

For a Herschel–Bulkley fluid of flow index N , the same features are observed in the plastically dominated regime, with the distinguished scaling given instead by $\epsilon = Bi^{-1/(N+1)}$ and the radial dependence of the boundary layer width given by $\epsilon r^{-2N/(N+1)}$ for flow in a wedge. We choose not to explore in detail, in this paper, the problem of a Herschel–Bulkley fluid in an axisymmetric conical geometry in the plastically dominated regime ($Bi \gg 1$). However, we can deduce by simple scaling arguments, analogous to those in §§ 5, 6, that the boundary layer width scales as $(r^{3N} Bi)^{-1/(N+1)}$, where N is the flow index. Notably, the boundary layer is of constant Cartesian thickness for the flow of a Bingham material through a wedge and for a Herschel–Bulkley fluid of flow index $N = 1/2$ through a cone, but not for the other situations.

In the viscously dominated regime ($Bi \ll 1$), the weak angular flow is $O(Bi)$ and, in contrast to the plastically dominated regime, is stronger for larger half-angles. This is due to the leading-order viscous flow shearing the fluid less strongly for larger half-angles, resulting in less strongly yielded fluid and a more significant effect of the yield stress. The shear stress at the wall is again enhanced compared to the purely viscous solution, with the excess shear stress being $O(Bi)$.

The direct finite element simulations, carried out in FEniCS (Alnæs *et al.* 2015) using a combination of augmented-Lagrangian and Newton methods, strongly supported the validity of the asymptotic solutions derived in the case of a Bingham fluid in a planar wedge. Boundary layer widths and velocity profiles were found to be in excellent agreement with the theoretical results. The challenges posed by the converging geometry and nonlinear constitutive equation leave room for a more expansive and accurate numerical study. In particular, we were unable to reproduce accurately the predictions for both the plastic and viscous regimes in the same simulations due to the vastly disparate scales involved in the different regimes.

This study has tackled the simplest and most generic scenario for converging flows of viscoplastic materials, demonstrating the emergence of viscoplastic boundary layers when the viscous stresses are weak, and the development of an angular flow. It would be interesting to analyse the motion in related problems, such as those driven by a body force (e.g. gravity) or situations in which there is wall slip or significant inertia.

There have been several experimental investigations of extrusions and flows through dies and contractions (for e.g. Wildman *et al.* 1999; Jay, Magnin & Piau 2002; Rabideau *et al.* 2010; Luu, Philippe & Chambon 2015), but the authors are unaware of any experimental observations that may be used to validate the predictions of this theory. In particular it would be interesting to detect and quantify experimentally the emergent angular flow predicted by our analysis.

Funding. This work was funded by the Engineering and Physical Sciences Research Council, UK. (EP/R513179/1).

Declaration of interests. The authors report no conflict of interest.

Author ORCIDs.

 Jesse J. Taylor-West <https://orcid.org/0000-0002-7511-1894>;

 Andrew J. Hogg <https://orcid.org/0000-0002-9387-6698>.

Appendix A

Expansion of the equation for ψ_0 , (3.11), for $1 - \Theta \ll 1$ gives

$$\psi_0 = \frac{\pi}{4} - \sqrt{\alpha c (1 - \Theta)} + \frac{2}{3}\alpha (1 - \Theta) + \dots \quad (\text{A1})$$

Substituting this into the definitions of the scaled radial velocity, \hat{u}_0 , (3.12), and the components of deviatoric stress, τ_{rr} and $\tau_{r\theta}$, (3.2), gives

$$\hat{u}_0 = -\frac{A}{c} - \frac{2A}{c} \sqrt{\frac{\alpha}{c} (1 - \Theta)} - \frac{8A\alpha}{3c^2} (1 - \Theta) + \dots, \quad (\text{A2})$$

$$\tau_{rr} \equiv Bi \cos 2\psi_0 = 2Bi\sqrt{\alpha c (1 - \Theta)} - \frac{4}{3}Bi\alpha (1 - \Theta) + \dots, \quad (\text{A3})$$

$$\tau_{r\theta} \equiv Bi \sin 2\psi_0 = Bi - 2Bi\alpha c (1 - \Theta) + \dots \quad (\text{A4})$$

Appendix B

For a Herschel–Bulkley fluid with flow index N , the generalisation of equations (3.46)–(3.48) is given by

$$\begin{aligned} & \frac{1}{\alpha^2} (\hat{\psi}_1 \cos 2\psi_0)'' + \frac{4}{(N+1)^2} \hat{\psi}_1 \cos 2\psi_0 - \frac{2(1-N)}{\alpha(1+N)} (\hat{\psi}_1 \sin 2\psi_0)' \\ &= \frac{\hat{\Phi}}{\alpha^2} \left(\frac{2N}{N+1} \Theta (\cos 2\psi_0)'' - \frac{1-N}{N+1} (\cos 2\psi_0)' - \frac{1}{\alpha} (\sin 2\psi_0)'' \right. \\ & \quad \left. - \frac{N}{N+1} \alpha \Theta (\sin 2\psi_0)' \right), \end{aligned} \quad (\text{B1})$$

$$-\frac{2N}{N+1} \hat{u}_1 + \frac{1}{\alpha} \hat{v}_1' = \frac{2N}{N+1} \frac{\hat{\Phi} \Theta}{\alpha} \hat{u}_0', \quad (\text{B2})$$

$$\begin{aligned} & -\frac{6N+2}{N+1} \hat{u}_1 \tan 2\psi_0 - \frac{1}{\alpha} \hat{u}_1' + \frac{4N+2}{N+1} \hat{v}_1 - 4\hat{\psi}_1 \hat{u}_0 \sec^2 2\psi_0 \\ &= \frac{\hat{\Phi}}{\alpha} \left(\frac{4N}{N+1} \Theta \tan 2\psi_0 + \frac{1}{\alpha} \right) \hat{u}_0', \end{aligned} \quad (\text{B3})$$

with boundary conditions

$$\hat{v}_1(0) = \hat{\psi}_0(0) = 0, \quad \hat{v}_1(1) = -\frac{2N^3}{(2N+1)(N+1)^2} \hat{\phi}^{2+1/N} (2c)^{1/N}, \quad (\text{B4a,b})$$

where $\hat{\phi}$ is given by (3.15) and c and A are given by (3.14) and (3.15). When $N = 1$ we have $\hat{\phi} = \sqrt{A}/c$ and the equations reduce to (3.46)–(3.48), as required.

The boundary condition for $\hat{\psi}_1$ at $\Theta = 1$ can be deduced by matching the deviatoric normal stress, τ_{rr} , between the bulk and intermediate layer, as detailed for the Bingham case in § 3.5. This gives

$$\hat{\psi}_1(1) = \frac{2N}{N+1} \hat{\phi}. \quad (\text{B5})$$

Using (A1) and (A2), we analyse the limiting behaviour of the equations (B1)–(B3) for $|1 - \Theta| \ll 1$, which yields the following local forms of all three dependent variables:

$$\hat{\psi}_1 = \frac{2N}{N+1} \hat{\phi} + E \sqrt{\frac{\alpha}{c} (1 - \Theta)} + \dots, \quad (\text{B6})$$

$$\hat{u}_1 = F + \left(\frac{6N+2}{N+1} F + \frac{2A}{c^2} \left(\frac{c\hat{\phi}}{\alpha} - E \right) \right) \sqrt{\frac{\alpha}{c} (1 - \Theta)} + \dots \quad (\text{B7})$$

$$\hat{v}_1 = -\frac{2N^3 \hat{\phi}^{2+1/N}}{(2N+1)(N+1)^2} (2c)^{1/N} - \frac{4N}{N+1} \frac{A\hat{\phi}}{c} \sqrt{\frac{\alpha}{c} (1 - \Theta)} + \dots, \quad (\text{B8})$$

where E and F are arbitrary constants.

Appendix C

Expansion of the differential equation for ψ_0 , (6.26), at $\Theta = 1$ gives the asymptotic series

$$\psi_0 = \frac{\pi}{4} - \sqrt{\frac{\alpha}{2} (2c - \cot \alpha) (1 - \Theta)} + \frac{2\sqrt{3}}{3} \alpha (1 - \Theta) + \dots \quad (\text{C1})$$

Matching the leading-order radial velocity to the intermediate and boundary layers gives

$$\hat{u}_0(\Theta = 1) = -c\hat{\phi}^2, \quad (\text{C2})$$

and expansion of the leading-order solution, (6.25a,b), gives

$$\hat{u}_0 = -c\hat{\phi}^2 \left(1 + \frac{2\sqrt{6}}{\sqrt{2c - \cot \alpha}} \sqrt{\alpha (1 - \Theta)} + \frac{16\alpha}{2c - \cot \alpha} (1 - \Theta) + \dots \right). \quad (\text{C3})$$

The converging flow of viscoplastic fluid

Then, analysis of the first-order equations, (6.31)–(6.34), and application of boundary conditions, (6.35a,b) and (6.36), reveals that solutions have the local form

$$\hat{\psi}_1 = \frac{3\sqrt{3}}{4}\hat{\phi} + \mathcal{E}\sqrt{1-\Theta} + \dots, \tag{C4}$$

$$\hat{u}_1 = \mathcal{F} + \left(\frac{7\sqrt{6\alpha}}{2\sqrt{2c-\cot\alpha}}\mathcal{F} + c\hat{\phi}^2 \left(\frac{\sqrt{6}\hat{\phi}}{\sqrt{\alpha}(2c-\cot\alpha)} - \frac{2\sqrt{3}\mathcal{E}}{(2c-\cot\alpha)^{3/2}} \right) \right) \sqrt{1-\Theta} + \dots, \tag{C5}$$

$$\hat{v}_1 = -\frac{c\hat{\phi}^3}{3} \left(1 + \frac{9\sqrt{6}}{\sqrt{2c-\cot\alpha}}\sqrt{\alpha(1-\Theta)} + \dots \right), \tag{C6}$$

where \mathcal{E} and \mathcal{F} are undetermined constants. We note that $\hat{\chi}_1$ is in fact determined algebraically by (6.34), so we require no boundary conditions for $\hat{\chi}_1$. To leading order at $\Theta = 1$ we have

$$\hat{\chi}_1 = \frac{3\sqrt{2}\hat{\phi}}{8\sqrt{\alpha}(2c-\cot\alpha)(1-\Theta)} + \dots, \tag{C7}$$

as required for matching of the normal stress difference between the intermediate layer and bulk solution, (6.37) and (6.38).

For $\Theta \ll 1$ we have the leading-order local forms

$$\hat{\psi}_0 = \frac{\alpha(c-\sqrt{3})}{2}\Theta + \dots, \quad \hat{u}_0 = -\mathcal{A} + \dots, \quad \hat{\psi}_1 = \tilde{\mathcal{E}}\Theta + \dots, \quad \hat{u}_1 = \tilde{\mathcal{F}} + \dots, \tag{C8a-d}$$

where $\tilde{\mathcal{E}}$ and $\tilde{\mathcal{F}}$ are undetermined constants.

Appendix D

For small Bingham number, $Bi \ll 1$, we consider the plane Poiseuille flow of a Bingham fluid in a channel of height 2 and volume flux per unit width -1 , driven by pressure gradient $dp/dx = G$. From the volume-flux condition we can write

$$\begin{aligned} -\frac{1}{2} &= \int_0^1 u \, dy = u_p y_c + \int_{y_c}^1 u \, dy = -\int_{y_c}^1 y \frac{du}{dy} \, dy = -\int_{y_c}^1 y(Gy - Bi) \, dy \\ &= -\frac{G}{3} + \frac{1}{2}Bi + \dots, \end{aligned} \tag{D1}$$

where u_p is the velocity of the plug which occupies the region $-y_c < y < y_c$. In the above we have used integration by parts, made the substitution $du/dy = Gy - Bi$, using the integral of the streamwise conservation of momentum equation in the yielded region, and finally used the fact that $y_c = O(Bi)$ in neglecting terms in the final expression.

Thus we find

$$G = \frac{3}{2} + \frac{3}{2}Bi + \dots, \quad (D2)$$

and, by a global force balance, the shear stress at the wall is given by

$$\tau_{xy} = G = \frac{3}{2} + \frac{3}{2}Bi + \dots \quad (D3)$$

Similarly, for the pipe Poiseuille flow of a Bingham fluid along the axis of a cylinder of unit radius, with volume flux -1 driven by a pressure gradient $dp/dz = G$, we can write

$$\begin{aligned} -1 &= 2\pi \int_0^1 ru \, dr = \pi r_c^2 u_p + 2\pi \int_{r_c}^1 ru \, dr = -\pi \int_{r_c}^1 r^2 \left(\frac{1}{2}Gr - Bi \right) dr \\ &= -\frac{\pi}{8}G + \frac{\pi}{3}Bi + \dots, \end{aligned} \quad (D4)$$

and so

$$G = \frac{8}{\pi} + \frac{8}{3}Bi + \dots, \quad (D5)$$

and, by a global force balance, the shear stress at the wall is given by

$$\tau_{rz} = \frac{1}{2}G = \frac{4}{\pi} + \frac{4}{3}Bi + \dots \quad (D6)$$

REFERENCES

- ACKERBERG, R.C. 1965 The viscous incompressible flow inside a cone. *J. Fluid Mech.* **21** (1), 47–81.
- ALEXANDROV, S., LYAMINA, E. & MISHURIS, G. 2007 Flow of viscoplastic materials through converging channels. *Proc. Appl. Maths Mech.* **7** (1), 1060603–1060604.
- ALNÆS, M.S., BLECHTA, J., HAKE, J., JOHANSSON, A., KEHLET, B., LOGG, A., RICHARDSON, C., RING, J., ROGNES, M.E. & WELLS, G.N. 2015 The FEniCS project version 1.5. *Arch. Numer. Softw.* **3** (100), 9–23.
- ANCEY, C. 2007 Plasticity and geophysical flows: a review. *J. Non-Newtonian Fluid Mech.* **142** (1–3), 4–35.
- ARA, A., KHAN, N., SULTAN, F. & ULLAH, S. 2019 Numerical simulation of Jeffery–Hamel flow of Bingham plastic fluid and heat transfer in the presence of magnetic field. *Appl. Comput. Maths* **18**, 135–148.
- BALMFORTH, N.J. & CRASTER, R.V. 1999 A consistent thin-layer theory for Bingham plastics. *J. Non-Newtonian Fluid Mech.* **84** (1), 65–81.
- BALMFORTH, N.J., CRASTER, R.V., HEWITT, D.R., HORMOZI, S. & MALEKI, A. 2017 Viscoplastic boundary layers. *J. Fluid Mech.* **813**, 929–954.
- BALMFORTH, N.J., FRIGAARD, I.A. & OVARLEZ, G. 2014 Yielding to stress: recent developments in viscoplastic fluid mechanics. *Annu. Rev. Fluid Mech.* **46** (1), 121–146.
- BANKS, W.H.H., DRAZIN, P.G. & ZATURSKA, M.B. 1988 On perturbations of Jeffery–Hamel flow. *J. Fluid Mech.* **186**, 559–581.
- BREWSTER, M.E., CHAPMAN, S.J., FITT, A.D. & PLEASE, C.P. 1995 Asymptotics of slow flow of very small exponent power-law shear-thinning fluids in a wedge. *Eur. J. Appl. Maths* **6** (6), 559–571.
- CRISTESCU, N. 1975 Plastic flow through conical converging dies, using a viscoplastic constitutive equation. *Intl J. Mech. Sci.* **17** (6), 425–433.
- DEAN, W.R. 1934 Note on the divergent flow of fluid. *Lond. Edinb. Dubl. Phil. Mag. J. Sci.* **18** (121), 759–777.
- DRAZIN, P.G. & RILEY, N. 2006 *The Navier–Stokes Equations: A Classification of Flows and Exact Solutions*. Cambridge University Press.
- DURBAN, D. 1984 Rate effects in steady forming processes of plastic materials. *Intl J. Mech. Sci.* **26** (4), 293–304.
- DURBAN, D. 1985 On some simple steady forming process of viscoplastic solids. *Acta Mechanica* **57** (3), 123–141.
- DURBAN, D. 1986 On generalized radial flow patterns of viscoplastic solids with some applications. *Intl J. Mech. Sci.* **28** (2), 97–110.
- FRAENKEL, L.E. 1962 Laminar flow in symmetrical channels with slightly curved walls. I. On the Jeffery–Hamel solutions for flow between plane walls. *Proc. R. Soc. Lond. A* **267** (1328), 119–138.

The converging flow of viscoplastic fluid

- FRIGAARD, I.A., PASO, K. & DE SOUZA MENDES, P.R. 2017 Bingham's model in the oil and gas industry. *Rheol. Acta* **56**, 259–282.
- HAMEL, G. 1917 Spiralförmige Bewegungen zäher Flüssigkeiten. *Jahresbericht der Deutschen Mathematiker-Vereinigung* **25**, 34–60.
- HARRISON, W.J. 1919 The pressure in a viscous liquid moving through a channel with diverging boundaries. *Proc. Camb. Phil. Soc.* **19**, 307–312.
- HILL, R. 1950 *The Mathematical Theory of Plasticity*. Clarendon Press.
- HULL, A.M. & PEARSON, J.R.A. 1984 On the converging flow of viscoelastic fluids through cones and wedges. *J. Non-Newtonian Fluid Mech.* **14**, 219–247.
- JAY, P., MAGNIN, A. & PIAU, J.M. 2002 Numerical simulation of viscoplastic fluid flows through an axisymmetric contraction. *Trans. ASME: J. Fluids Engng* **124** (3), 700–705.
- JEFFERY, G.B. 1915 The two-dimensional steady motion of a viscous fluid. *Lond. Edinb. Dubl. Phil. Mag. J. Sci.* **29** (172), 455–465.
- LOGG, A., MARDAL, K.-A. & WELLS, G.N. 2012 *Automated Solution of Differential Equations by the Finite Element Method*. Springer.
- LUU, L.-H., PHILIPPE, P. & CHAMBON, G. 2015 Experimental study of the solid-liquid interface in a yield-stress fluid flow upstream of a step. *Phys. Rev. E* **91**, 013013.
- NADAI, A. 1924 Über die Gleit- und Verzweigungsflächen einiger Gleichgewichtszustände bildsamer Massen und die Nachspannungen bleibend verzerrter Körper. *Z. Phys.* **30**, 106–138.
- NAGLER, J. 2017 Jeffery–Hamel flow of non-Newtonian fluid with nonlinear viscosity and wall friction. *Z. Angew. Math. Mech.* **38**, 815–830.
- OLDROYD, J.G. 1947 Two-dimensional plastic flow of a Bingham solid: a plastic boundary-layer theory for slow motion. *Math. Proc. Cambridge* **43** (3), 383–395.
- PIAU, J.-M. 2002 Viscoplastic boundary layer. *J. Non-Newtonian Fluid Mech.* **102** (2), 193–218.
- PIAU, J.-M. & DEBIANE, K. 2004 The adhesive or slippery flat plate viscoplastic boundary layer for a shear-thinning power-law viscosity. *J. Non-Newtonian Fluid Mech.* **117** (2), 97–107.
- RABIDEAU, B.D., MOUCHERONT, P., BERTRAND, F., RODTS, S., ROUSSEL, N., LANOS, C. & COUSSOT, P. 2010 The extrusion of a model yield stress fluid imaged by MRI velocimetry. *J. Non-Newtonian Fluid Mech.* **165** (7), 394–408.
- ROSENHEAD, L. 1940 The steady two-dimensional radial flow of viscous fluid between two inclined plane walls. *Proc. R. Soc. Lond. A* **175** (963), 436–467.
- SANDRU, N. & CAMENSHI, C. 1979 Viscoplastic flow through inclined planes with application to the strip drawing. *Intl J. Engng Sci.* **17** (6), 773–784.
- SARAMITO, P. 2016 Complex fluids: modeling and algorithms. In *Viscoplastic Fluids*, 91–142. Springer.
- SHIELD, R.T. 1955 Plastic flow in a converging conical channel. *J. Mech. Phys. Solids* **3** (4), 246–258.
- TOKPAVI, D.L., MAGNIN, A. & JAY, P. 2008 Very slow flow of Bingham viscoplastic fluid around a circular cylinder. *J. Non-Newtonian Fluid Mech.* **154** (1), 65–76.
- WALTON, I.C. & BITTLESTON, S.H. 1991 The axial flow of a Bingham plastic in a narrow eccentric annulus. *J. Fluid Mech.* **222**, 39–60.
- WILDMAN, R.D., BLACKBURN, S., BENTON, D.M., MCNEIL, P.A. & PARKER, D.J. 1999 Investigation of paste flow using positron emission particle tracking. *Powder Technol.* **103** (3), 220–229.